

An interface/boundary-unfitted eXtended HDG method for linear elasticity problems*

Yihui Han[†], Xiao-Ping Wang[‡], Xiaoping Xie[§]

Abstract

An interface/boundary-unfitted eXtended hybridizable discontinuous Galerkin (X-HDG) method of arbitrary order is proposed for linear elasticity interface problems on unfitted meshes with respect to the interface and domain boundary. The method uses piecewise polynomials of degrees k (≥ 1) and $k - 1$ respectively for the displacement and stress approximations in the interior of elements inside the subdomains separated by the interface, and piecewise polynomials of degree k for the numerical traces of the displacement on the inter-element boundaries inside the subdomains and on the interface/boundary of the domain. Optimal error estimates in L^2 -norm for the stress and displacement are derived, which are uniform with respect to the Lamé constant λ . Finally, numerical experiments confirm the theoretical results and show that the method also applies to the case of crack-tip domain.

Key Words: eXtended HDG method, linear elasticity, interface/boundary-unfitted, error estimate, crack-tip domain

1 Introduction

Let $\Omega \subset \mathbb{R}^d$ ($d = 2, 3$) be a bounded domain with piecewise smooth boundary $\partial\Omega = \partial\Omega_D \cup \partial\Omega_N$, where $\text{meas}(\partial\Omega_D) > 0$ and $\partial\Omega_D \cap \partial\Omega_N = \emptyset$. The domain Ω is divided into two subdomains, Ω_i ($i = 1, 2$), by a piecewise smooth interface Γ (cf. Figure 1 for an example). Consider the linear elasticity interface problem

$$\mathcal{A}\boldsymbol{\sigma} - \boldsymbol{\epsilon}(\mathbf{u}) = \mathbf{0} \quad \text{in } \Omega_1 \cup \Omega_2, \quad (1.1a)$$

$$\nabla \cdot \boldsymbol{\sigma} = \mathbf{f} \quad \text{in } \Omega_1 \cup \Omega_2, \quad (1.1b)$$

$$\mathbf{u} = \mathbf{g}_D \quad \text{on } \partial\Omega_D, \quad (1.1c)$$

$$\boldsymbol{\sigma}\mathbf{n} = \mathbf{g}_N \quad \text{on } \partial\Omega_N, \quad (1.1d)$$

$$[[\mathbf{u}]] = \mathbf{0}, \quad [[\boldsymbol{\sigma}\mathbf{n}]] = \mathbf{g}_N^\Gamma \quad \text{on } \Gamma, \quad (1.1e)$$

where $\boldsymbol{\sigma} : \Omega \rightarrow \mathbb{R}_{sym}^{d \times d}$ denotes the symmetric $d \times d$ stress tensor field, $\mathbf{u} : \Omega \rightarrow \mathbb{R}^d$ the displacement field, $\boldsymbol{\epsilon}(\mathbf{u}) = (\nabla\mathbf{u} + (\nabla\mathbf{u})^T)/2$ the strain tensor, and $\mathcal{A} \in \mathbb{R}_{sym}^{d \times d}$ the compliance tensor with

$$\mathcal{A}\boldsymbol{\sigma} = \frac{1}{2\mu} \left(\boldsymbol{\sigma} - \frac{\lambda}{2\mu + d\lambda} \text{tr}(\boldsymbol{\sigma})\mathbf{I} \right). \quad (1.2)$$

Here $\text{tr}(\boldsymbol{\sigma})$ denotes the trace of $\boldsymbol{\sigma}$, \mathbf{I} the $d \times d$ identity matrix, and λ and μ the Lamé coefficients with $\lambda|_{\Omega_i} = \lambda_i > 0$ and $\mu|_{\Omega_i} = \mu_i > 0$. \mathbf{f} is the body force, \mathbf{g}_D and \mathbf{g}_N are respectively the surface displacement on $\partial\Omega_D$ and the surface traction on $\partial\Omega_N$, and \mathbf{n} in (1.1d) and (1.1e) denotes respectively the unit outer normal vector along $\partial\Omega_N$ and the unit normal vector along Γ pointing to Ω_2 . The jump

*This work was supported in part by National Natural Science Foundation of China (11771312).

[†]South China Research Center for Applied Mathematics and Interdisciplinary Studies, South China Normal University, Guangzhou, 510630, China, Email: yhhan@m.scnu.edu.cn

[‡]Department of Mathematics, The Hong Kong University of Science and Technology, Clear Water Bay, Kowloon, Hong Kong, China, Email: mawang@ust.hk

[§]Corresponding author. School of Mathematics, Sichuan University, Chengdu, 610064, China, Email: xpxie@scu.edu.cn

of a function w across the interface Γ is defined by $[[w]] = (w|_{\Omega_1})|_{\Gamma} - (w|_{\Omega_2})|_{\Gamma}$. Elasticity interface problems are usually used to describe complicated elasticity structure characterized by discontinuous or even singular material properties, and have many applications in materials science and continuum mechanics [29, 30, 39, 41, 54, 60, 63].

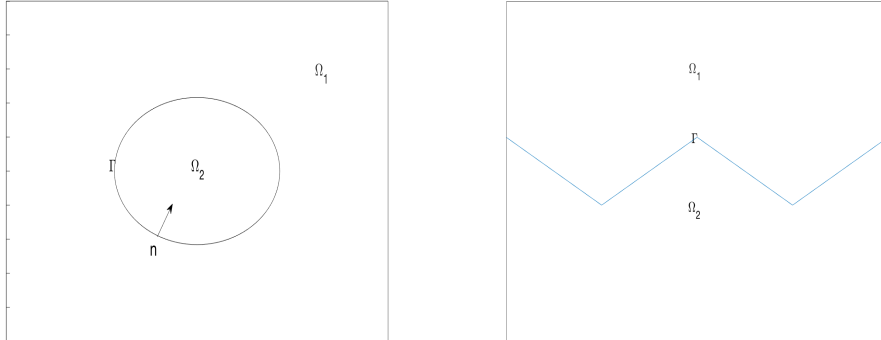


Figure 1: *The geometry of domain with circle interface or fold line interface*

For elliptic interface problems, the global regularity of the solutions is generally very low, which may lead to reduced accuracy of finite element discretizations [2, 68]. To tackle this situation there are mainly two types of methods in the literature: interface-fitted methods and interface-unfitted methods. The fitted methods use interface-fitted meshes to dominate the approximation error caused by the low regularity of solutions [6, 10, 13, 14, 18, 38, 47, 55]; see Figure 2 for an example. However, it is usually expensive to generate interface-fitted meshes, especially when the interface is of complicated geometry or moving with time or iteration.

The unfitted methods, based on meshes independent of the interface, employ certain types of modification in the finite element discretization for approximating functions around the interface so as to avoid the loss of numerical accuracy. One representative unfitted method is the eXtended/generalized Finite Element Method [3, 4, 8, 36, 40, 53, 62, 64, 65], where additional basis functions characterizing the solution singularity around the interface are adopted for the corresponding approximation function space. For elasticity interface problems, we refer to [37] for an XFEM of displacement-type, and to [7, 37] for a mixed XFEM based on a displacement-pressure formulation, both of which use the cut linear polynomials around the interface as additional basis functions to enrich the standard linear element displacement spaces. We also refer to [9, 28, 46, 58, 59] for some applications of XFEMs in the simulation of crack propagation in fracture mechanics and [11, 12, 32] for domain with curved boundary.

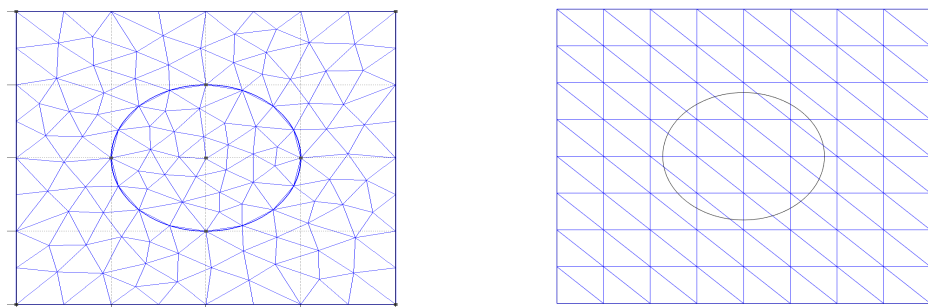


Figure 2: *Fitted mesh (left) and Unfitted mesh (right)*

The immersed finite element method (IFEM) is another type of interface-unfitted methods, where

special finite element basis functions are constructed to satisfy the interface jump conditions [1, 31, 42, 48, 49, 50, 56, 69]. We refer to [51, 52] for linear/bilinear immersed finite elements and a nonconforming immersed rectangular element for planar elasticity interface problems.

The hybridizable discontinuous Galerkin (HDG) framework [19] provides a unifying strategy for hybridization of finite element methods. In this framework, a trace variable defined on the mesh skeleton is introduced, as a Lagrange multiplier, so as to relax the continuity constraint of the approximation solution on the inter-element boundaries. Thus, the HDG method allows for local elimination of unknowns defined in the interior of elements and leads to a reduction of the number of degrees of freedom in the final discrete system. We refer to [16, 17, 20, 21, 23, 24, 43, 44, 45, 57] for some developments of the HDG method and [22, 25, 26, 61] for HDG method to deal with domain with curved boundary. In [27] an unfitted HDG method was developed for two-dimensional Poisson interface problems by constructing a novel ansatz function in the vicinity of the interface. Based on the XFEM philosophy and a level set description of interface, an equal order eXtended HDG (X-HDG) method was proposed in [34] for diffusion problems with voids and later applied to heat bimaterial problems [33]. In [35] two arbitrary order X-HDG methods with optimal convergence rates were presented and analyzed for diffusion interface problems in two and three dimensions.

This paper aims to develop an interface/boundary-unfitted X-HDG method of arbitrary order for the linear elasticity interface problem (1.1). The main features of our X-HDG method are as follows.

- The method uses piecewise polynomials of degrees k (≥ 1) and $k - 1$ respectively for the displacement and stress approximations in the interior of elements inside the subdomains separated by the interface, and piecewise polynomials of degree k for the numerical traces of the displacement on the inter-element boundaries inside the subdomains and on the interface/boundary of the domain. We note that the unfitted methods in [7, 37, 51, 52] are low order ones, and that the methods in [15, 57] for linear elasticity problems (without interface) use piecewise polynomials of degrees $k + 1$, k and k respectively for the displacement, stress approximations in the interior of elements and the numerical traces of displacement on the inter-element boundaries.
- The method inherits the following advantages of X-FEM and HDG: it does not require the used meshes to fit the interface or boundary; it has the property of local elimination; and it does not require the stabilization parameters to be sufficiently large .
- The derived error estimates are optimal and uniform with respect to the Lamé constant λ .
- The method applies to any piecewise C^2 smooth interface and any crack-tip domain.

The rest of the paper is organized as follows. Section 2 introduces the X-HDG scheme for the elasticity problem on interface-unfitted meshes and boundary-unfitted meshes, respectively. Section 3 is devoted to the a priori error estimation for the X-HDG method. Finally, numerical examples are provided in Section 4 to verify the theoretical results.

2 X-HDG scheme

2.1 Notation

For any bounded polygonal/polyhedral domain $D \subset \mathbb{R}^s$ ($s = d, d - 1$) and nonnegative integer m , let $H^m(D)$ and $H_0^m(D)$ be the usual m -th order Sobolev spaces on D , with norm $\|\cdot\|_{m,D}$ and semi-norm $|\cdot|_{m,D}$. In particular, $L^2(D) := H^0(D)$ is the space of square integrable functions, with the inner product $(\cdot, \cdot)_D$. When $D \subset \mathbb{R}^{d-1}$, we use $\langle \cdot, \cdot \rangle_D$ to replace $(\cdot, \cdot)_D$. We set

$$H^m(\Omega_1 \cup \Omega_2) := \{v \in L^2(\Omega), v|_{\Omega_1} \in H^m(\Omega_1), \text{ and } v|_{\Omega_2} \in H^m(\Omega_2)\},$$

$$\|\cdot\|_m := \|\cdot\|_{m, \Omega_1 \cup \Omega_2} = \sum_{i=1}^2 \|\cdot\|_{m, \Omega_i}, \quad |\cdot|_m := |\cdot|_{m, \Omega_1 \cup \Omega_2} = \sum_{i=1}^2 |\cdot|_{m, \Omega_i}.$$

For integer $k \geq 0$, $P_k(D)$ denotes the set of all polynomials on D with degree no more than k . We note that bold face fonts will be used for vector (or tensor) analogues of the Sobolev spaces along with vector-valued (or tensor-valued) functions.

Let $\mathcal{T}_h = \cup\{K\}$ be a shape-regular triangulation of the domain Ω consisting of open triangles/tetrahedrons, which is unfitted with the interface. We define the set of all elements intersected by the interface Γ as

$$\mathcal{T}_h^\Gamma := \{K \in \mathcal{T}_h : K \cap \Gamma \neq \emptyset\}.$$

For any $K \in \mathcal{T}_h^\Gamma$ which is called an interface element, let $\Gamma_K := K \cap \Gamma$ be the part of Γ in K , $K_i = K \cap \Omega_i$ be the part of K in Ω_i ($i = 1, 2$), and $\Gamma_{K,h}$ be the straight line/plane segment connecting the intersection between Γ_K and ∂K . To ensure that Γ is reasonably resolved by \mathcal{T}_h , we make the following standard assumptions on \mathcal{T}_h and interface Γ :

(A1). For $K \in \mathcal{T}_h^\Gamma$ and any edge/face $F \subset \partial K$ which intersects Γ , $F_\Gamma := \Gamma \cap F$ is simply connected with either $F_\Gamma = F$ or $meas(F_\Gamma) = 0$.

(A2). For $K \in \mathcal{T}_h^\Gamma$, there is a smooth function ψ which maps $\Gamma_{K,h}$ onto Γ_K .

(A3). For any two different points $\mathbf{x}, \mathbf{y} \in \Gamma_K$, the unit normal vectors $\mathbf{n}(\mathbf{x})$ and $\mathbf{n}(\mathbf{y})$, pointing to Ω_2 , at \mathbf{x} and \mathbf{y} satisfy

$$|\mathbf{n}(\mathbf{x}) - \mathbf{n}(\mathbf{y})| \leq \gamma h_K, \quad (2.1)$$

with $\gamma \geq 0$ (cf. [18, 68]). Note that $\gamma = 0$ when Γ_K is a straight line/plane segment.

Let ε_h be the set of all edges (faces) of all elements in \mathcal{T}_h and ε_h^Γ be the partition of Γ with respect to \mathcal{T}_h , i.e.

$$\varepsilon_h^\Gamma := \{F : F = \Gamma_K, \text{ or } F = \Gamma \cap \partial K \text{ if } \Gamma \cap \partial K \text{ is an edge/face of } K, \forall K \in \mathcal{T}_h\},$$

and set $\varepsilon_h^* := \varepsilon_h \setminus \varepsilon_h^\Gamma$. For any $K \in \mathcal{T}_h$ and $F \in \varepsilon_h^* \cup \varepsilon_h^\Gamma$, h_K and h_F denote respectively the diameters of K and F , and \mathbf{n}_K denotes the unit outward normal vector along ∂K . We denote by $h := \max_{K \in \mathcal{T}_h} h_K$ the mesh size of \mathcal{T}_h , and by ∇_h and $\nabla_h \cdot$ the piecewise-defined gradient and divergence operators with respect to \mathcal{T}_h , respectively.

Throughout the paper, we use $a \lesssim b$ ($a \gtrsim b$) to denote $a \leq Cb$ ($a \geq Cb$), where C is a generic positive constant independent of mesh parameters h, h_K, h_e , the coefficients μ_i, λ_i ($i = 1, 2$) and the location of the interface relative to the mesh.

2.2 X-HDG scheme on interface-unfitted meshes

For $i = 1, 2$, let χ_i be the characteristic function on Ω_i , and for any $K \in \mathcal{T}_h$, $F \in \varepsilon_h^* \cup \varepsilon_h^\Gamma$ and integer $r \geq 0$, let $Q_r^b : L^2(D) \rightarrow P_r(D)$ be the standard L^2 orthogonal projection operator with $D = F \cap \Omega_i$. And Let $Q_r : L^2(D) \rightarrow P_r(D)$ be the standard L^2 orthogonal projection operator with $D = K \cap \Omega_i$ for $i = 1, 2$. Vector or tensor analogues of Q_r^b and Q_r are denoted by \mathbf{Q}_r^b and \mathbf{Q}_r , respectively.

Set

$$\oplus \chi_i P_r(K) := \chi_1 P_r(K) + \chi_2 P_r(K), \quad \mathbf{L}^2(\Omega, S) := \{\mathbf{w} \in [L^2(\Omega)]^{d \times d} : \mathbf{w}^T = \mathbf{w}\}.$$

We introduce the following X-HDG finite element spaces:

$$\mathbf{W}_h = \{\mathbf{w} \in \mathbf{L}^2(\Omega, S) : \mathbf{w}|_K \in \mathbf{P}_{k-1}(K) \text{ if } K \cap \Gamma = \emptyset; \mathbf{w}|_K \in \oplus \chi_i \mathbf{P}_{k-1}(K) \text{ if } K \cap \Gamma \neq \emptyset\},$$

$$\mathbf{V}_h = \{\mathbf{v} \in \mathbf{L}^2(\Omega) : \mathbf{v}|_K \in \mathbf{P}_k(K) \text{ if } K \cap \Gamma = \emptyset; \mathbf{v}|_K \in \oplus \chi_i \mathbf{P}_k(K) \text{ if } K \cap \Gamma \neq \emptyset\},$$

$$\mathbf{M}_h = \{\hat{\boldsymbol{\mu}} \in \mathbf{L}^2(\varepsilon_h^*) : \forall F \in \varepsilon_h^*, \hat{\boldsymbol{\mu}}|_F \in \mathbf{P}_k(F) \text{ if } F \cap \Gamma = \emptyset; \hat{\boldsymbol{\mu}}|_F \in \oplus \chi_i \mathbf{P}_k(F) \text{ if } F \cap \Gamma \neq \emptyset\},$$

$$\tilde{\mathbf{M}}_h = \{\tilde{\boldsymbol{\mu}} \in \mathbf{L}^2(F) : \tilde{\boldsymbol{\mu}}|_F \in \mathbf{P}_k(K)|_F, \forall F \in \varepsilon_h^\Gamma\},$$

$$\mathbf{M}_h(\mathbf{g}_D) = \{\hat{\boldsymbol{\mu}} \in \mathbf{M}_h : \hat{\boldsymbol{\mu}}|_{\partial \Omega_D} = \mathbf{Q}_k^b \mathbf{g}_D\}.$$

Then the X-HDG method is given as follows: seek $(\boldsymbol{\sigma}_h, \mathbf{u}_h, \hat{\mathbf{u}}_h, \tilde{\mathbf{u}}_h) \in \mathbf{W}_h \times \mathbf{V}_h \times \mathbf{M}_h(\mathbf{g}_D) \times \tilde{\mathbf{M}}_h$ such

that

$$(\mathcal{A}\boldsymbol{\sigma}_h, \mathbf{w})_{\mathcal{T}_h} + (\mathbf{u}_h, \nabla_h \cdot \mathbf{w})_{\mathcal{T}_h} - \langle \hat{\mathbf{u}}_h, \mathbf{w}\mathbf{n} \rangle_{\partial\mathcal{T}_h \setminus \varepsilon_h^\Gamma} - \langle \tilde{\mathbf{u}}_h, \mathbf{w}\mathbf{n} \rangle_{*,\Gamma} = 0, \quad (2.2a)$$

$$(\nabla_h \cdot \boldsymbol{\sigma}_h, \mathbf{v})_{\mathcal{T}_h} - \langle \tau(\mathbf{u}_h - \hat{\mathbf{u}}_h), \mathbf{v} \rangle_{\partial\mathcal{T}_h \setminus \varepsilon_h^\Gamma} - \langle \eta(\mathbf{u}_h - \tilde{\mathbf{u}}_h), \mathbf{v} \rangle_{*,\Gamma} = (\mathbf{f}, \mathbf{v}), \quad (2.2b)$$

$$\langle \boldsymbol{\sigma}_h \mathbf{n}, \hat{\boldsymbol{\mu}} \rangle_{\partial\mathcal{T}_h \setminus \varepsilon_h^\Gamma} - \langle \tau(\mathbf{u}_h - \hat{\mathbf{u}}_h), \hat{\boldsymbol{\mu}} \rangle_{\partial\mathcal{T}_h \setminus \varepsilon_h^\Gamma} = \langle \mathbf{g}_N, \hat{\boldsymbol{\mu}} \rangle_{\partial\mathcal{T}_h \setminus \varepsilon_h^\Gamma}, \quad (2.2c)$$

$$\langle \boldsymbol{\sigma}_h \mathbf{n}, \tilde{\boldsymbol{\mu}} \rangle_{*,\Gamma} - \langle \eta(\mathbf{u}_h - \tilde{\mathbf{u}}_h), \tilde{\boldsymbol{\mu}} \rangle_{*,\Gamma} = \langle \mathbf{g}_N^\Gamma, \tilde{\boldsymbol{\mu}} \rangle_{*,\Gamma} \quad (2.2d)$$

for all $(\mathbf{w}, \mathbf{v}, \hat{\boldsymbol{\mu}}, \tilde{\boldsymbol{\mu}}) \in \mathbf{W}_h \times \mathbf{V}_h \times \mathbf{M}_h(\mathbf{0}) \times \tilde{\mathbf{M}}_h$. Here

$$(\cdot, \cdot)_{\mathcal{T}_h} := \sum_{K \in \mathcal{T}_h} (\cdot, \cdot)_K, \quad \langle \cdot, \cdot \rangle_{\partial\mathcal{T}_h \setminus \varepsilon_h^\Gamma} := \sum_{K \in \mathcal{T}_h} \langle \cdot, \cdot \rangle_{\partial K},$$

and, for vectors $\boldsymbol{\mu}, \mathbf{v}$ and tensor \mathbf{w} with $\boldsymbol{\mu}_i = \boldsymbol{\mu}|_{F \cap \Omega_i}$, $\mathbf{v}_i = \mathbf{v}|_{F \cap \Omega_i}$ and $\mathbf{w}_i = \mathbf{w}|_{F \cap \Omega_i}$,

$$\langle \boldsymbol{\mu}, \mathbf{v} \rangle_{*,\Gamma} := \sum_{F \in \varepsilon_h^\Gamma} \int_F (\boldsymbol{\mu}_1 \cdot \mathbf{v}_1 + \boldsymbol{\mu}_2 \cdot \mathbf{v}_2) ds,$$

$$\langle \mathbf{w}\mathbf{n}, \mathbf{v} \rangle_{*,\Gamma} := \sum_{F \in \varepsilon_h^\Gamma} \int_F ((\mathbf{w}_1 \mathbf{n}_1) \cdot \mathbf{v}_1 + (\mathbf{w}_2 \mathbf{n}_2) \cdot \mathbf{v}_2) ds,$$

where \mathbf{n}_i denotes the unit normal vector along Γ pointing from Ω_i to Ω_j with $i, j = 1, 2$ and $i \neq j$. The stabilization functions τ and η are defined as below: for any $K \in \mathcal{T}_h$, $F \in \varepsilon_h^\Gamma$ and $i = 1, 2$,

$$\tau|_{F \cap \Omega_i} = 2\mu_i h_K^{-1}, \quad \text{for } F \in \partial\mathcal{T}_h \setminus \varepsilon_h^\Gamma \text{ and } F \cap \Omega_i \neq \emptyset, \quad (2.3a)$$

$$\eta|_{F \cap \Omega_i} = 2\mu_i h_K^{-1}, \quad \text{for } F = \Gamma_K \text{ or } F \subset \partial(K \cap \Omega_i). \quad (2.3b)$$

Theorem 2.1. *For $k \geq 1$, the X-HDG scheme (2.2) admits a unique solution $(\boldsymbol{\sigma}_h, \mathbf{u}_h, \hat{\mathbf{u}}_h, \tilde{\mathbf{u}}_h) \in \mathbf{W}_h \times \mathbf{V}_h \times \mathbf{M}_h(\mathbf{g}_D) \times \tilde{\mathbf{M}}_h$.*

Proof. Since the (2.2) is a linear square system, it suffices to show that if all of the given data vanish, i.e. $\mathbf{f} = \mathbf{g}_D = \mathbf{g}_N = \mathbf{g}_N^\Gamma = \mathbf{0}$, then we get the zero solution. Taking $(\mathbf{w}, \mathbf{v}, \boldsymbol{\mu}, \tilde{\boldsymbol{\mu}}) = (\boldsymbol{\sigma}_h, \mathbf{u}_h, \hat{\mathbf{u}}_h, \tilde{\mathbf{u}}_h)$ in (2.2) and adding these equations together, we have

$$(\mathcal{A}\boldsymbol{\sigma}_h, \boldsymbol{\sigma}_h)_{\mathcal{T}_h} + \langle \tau(\mathbf{u}_h - \hat{\mathbf{u}}_h), \mathbf{u}_h - \hat{\mathbf{u}}_h \rangle_{\partial\mathcal{T}_h \setminus \varepsilon_h^\Gamma} + \langle \eta(\mathbf{u}_h - \tilde{\mathbf{u}}_h), \mathbf{u}_h - \tilde{\mathbf{u}}_h \rangle_{*,\Gamma} = 0, \quad (2.4)$$

which, together with the relation

$$(\mathcal{A}\mathbf{w}, \mathbf{w})_{\mathcal{T}_h} = \left(\frac{1}{2\mu} (\mathbf{w} - \frac{1}{d} \text{tr}(\mathbf{w})I), \mathbf{w} - \frac{1}{d} \text{tr}(\mathbf{w})I \right)_{\mathcal{T}_h} + \left(\frac{1}{d(d\lambda + 2\mu)} \text{tr}(\mathbf{w}), \text{tr}(\mathbf{w}) \right)_{\mathcal{T}_h}, \quad \forall \mathbf{w} \in \mathbf{W}_h,$$

shows that

$$\begin{aligned} \boldsymbol{\sigma}_h &= \mathbf{0}, & \text{in } \mathcal{T}_h, \\ \mathbf{u}_h - \hat{\mathbf{u}}_h &= \mathbf{0}, & \text{on } \partial\mathcal{T}_h \setminus \varepsilon_h^\Gamma, \\ \{\mathbf{u}_h - \tilde{\mathbf{u}}_h\} &= \mathbf{0}, & \text{on } \Gamma. \end{aligned}$$

Here $\{\cdot\}$ is defined by $\{\mathbf{v}\} = \frac{1}{2}(\mathbf{v}_1 + \mathbf{v}_2)$ with $\mathbf{v}_i = \mathbf{v}|_{\Gamma \cap \Omega_i}$ for $i = 1, 2$. These relations, plus (2.2a) and integration by parts, yield

$$(\mathcal{A}\boldsymbol{\sigma}_h, \mathbf{w})_{\mathcal{T}_h} + (\nabla_h \mathbf{u}_h, \mathbf{w})_{\mathcal{T}_h} - \langle \mathbf{u}_h - \hat{\mathbf{u}}_h, \mathbf{w}\mathbf{n} \rangle_{\partial\mathcal{T}_h \setminus \varepsilon_h^\Gamma} - \langle \mathbf{u}_h - \tilde{\mathbf{u}}_h, \mathbf{w}\mathbf{n} \rangle_{*,\Gamma} = 0.$$

Taking $\mathbf{w}_h = \nabla_h \mathbf{u}_h$ in this relation leads to $\nabla_h \mathbf{u}_h = \mathbf{0}$. In view of $\hat{\mathbf{u}}_h = \mathbf{0}$ on $\partial\Omega_D$, we get $\mathbf{u}_h = \{\tilde{\mathbf{u}}_h\} = \mathbf{0}$. Thus, from $\llbracket \tilde{\mathbf{u}}_h \rrbracket = \mathbf{0}$ it follows

$$\boldsymbol{\sigma}_h = \mathbf{u}_h = \hat{\mathbf{u}}_h = \tilde{\mathbf{u}}_h = \mathbf{0}.$$

This completes the proof. ■

2.3 X-HDG scheme on boundary-unfitted meshes

In this subsection, we shall extend the X-HDG method in Section 2.1 to the case using boundary-unfitted meshes (cf. Figure 3 for an example). For simplicity, we consider the following linear elasticity problem:

$$\mathcal{A}\boldsymbol{\sigma} - \boldsymbol{\epsilon}(\mathbf{u}) = \mathbf{0}, \quad \text{in } \Omega, \quad (2.5a)$$

$$\nabla \cdot \boldsymbol{\sigma} = \mathbf{f}, \quad \text{in } \Omega, \quad (2.5b)$$

$$\mathbf{u} = \mathbf{g}_D, \quad \text{on } \partial\Omega_D, \quad (2.5c)$$

$$\boldsymbol{\sigma}\mathbf{n} = \mathbf{g}_N, \quad \text{on } \partial\Omega_N. \quad (2.5d)$$

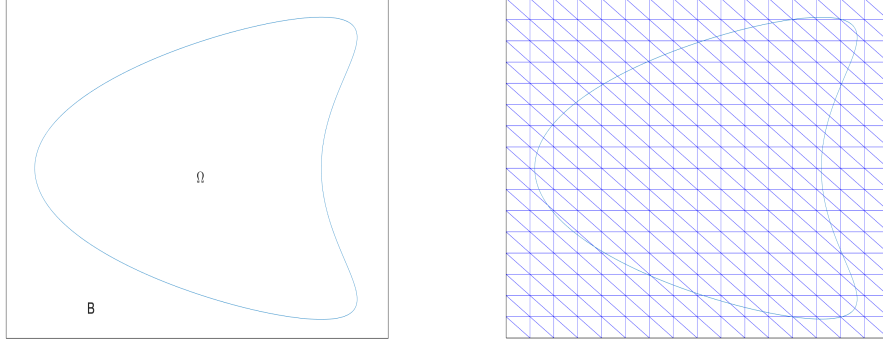


Figure 3: The geometry of domain with piecewise smooth boundary(left) and boundary unfitted mesh(right)

Let $\mathbb{B} \supset \Omega$ be a simpler domain than Ω (Figure 3), and denote $\Omega^c := \mathbb{B} \setminus \bar{\Omega}$. Then we can rewrite problem (2.5) as an interface problem:

$$\mathcal{A}\boldsymbol{\sigma} - \boldsymbol{\epsilon}(\mathbf{u}) = \mathbf{0}, \quad \text{in } \Omega \cup \Omega^c, \quad (2.6a)$$

$$\nabla \cdot \boldsymbol{\sigma} = \mathbf{f}, \quad \text{in } \Omega \cup \Omega^c, \quad (2.6b)$$

$$\mathbf{u} \equiv \mathbf{0}, \quad \boldsymbol{\sigma} \equiv \mathbf{0}, \quad \text{in } \Omega^c, \quad (2.6c)$$

$$[[\mathbf{u}]] = \mathbf{g}_D, \quad \text{on } \partial\Omega_D, \quad (2.6d)$$

$$[[\boldsymbol{\sigma}\mathbf{n}]] = \mathbf{g}_N, \quad \text{on } \partial\Omega_N. \quad (2.6e)$$

We note that the problem (2.6) is a special interface problem with $\partial\Omega$ being the interface, for which we only need to approximate the solution in Ω , since the solution in Ω^c is zero.

Let $\mathcal{T}_h = \cup\{K\}$ be a shape-regular triangulation of the domain \mathbb{B} consisting of open triangles/tetrahedrons. Define the following sets of elements and edges/faces:

$$\mathcal{T}_h^i := \{K \in \mathcal{T}_h : K \cap \Omega = K\},$$

$$\mathcal{T}_h^\Gamma := \{K_\Gamma : K_\Gamma = K \cap \Omega, K \in \mathcal{T}_h \text{ and } K \cap \partial\Omega \neq \emptyset\},$$

$$\mathcal{T}_h^* := \mathcal{T}_h^i \cup \mathcal{T}_h^\Gamma,$$

$$\varepsilon_h^i := \{F : F \text{ is a edge/face of element in } \mathcal{T}_h^i \text{ and } F \cap \partial\Omega = \emptyset\},$$

$$\varepsilon_h^\Gamma := \{F : F \text{ is a edge/face of element in } \mathcal{T}_h^\Gamma \text{ and } F \cap \partial\Omega = \emptyset\},$$

$$\varepsilon_h^\partial := \{F : F = K \cap \partial\Omega, \forall K \in \mathcal{T}_h^\Gamma \text{ or } F \text{ is a edge/face of } K, \forall K \in \mathcal{T}_h^i \text{ and } \bar{K} \cap \partial\Omega \neq \emptyset\},$$

$$\varepsilon_h := \varepsilon_h^i \cup \varepsilon_h^\Gamma \cup \varepsilon_h^\partial.$$

And introduce the following X-HDG finite element spaces:

$$\begin{aligned}
\mathbf{W}_h &:= \{\mathbf{w} \in \mathbf{L}^2(S, \Omega) : \mathbf{w}|_K \in \mathbf{P}_{k-1}(K) \text{ if } K \in \mathcal{T}_h^*\}, \\
\mathbf{V}_h &:= \{\mathbf{v} \in \mathbf{L}^2(\Omega) : \mathbf{v}|_K \in \mathbf{P}_k(K) \text{ if } K \in \mathcal{T}_h^*\}, \\
\mathbf{M}_h^i &:= \{\boldsymbol{\mu} \in \mathbf{L}^2(\varepsilon_h \setminus \varepsilon_h^\partial) : \boldsymbol{\mu}|_F \in \mathbf{P}_k(F) \text{ if } F \in \varepsilon_h \setminus \varepsilon_h^\partial\}, \\
\mathbf{M}_h^\partial &:= \{\tilde{\boldsymbol{\mu}} \in \mathbf{L}^2(\varepsilon_h^\partial) : \tilde{\boldsymbol{\mu}}|_F \in \mathbf{P}_k(K)|_F, \forall F \in \varepsilon_h^\partial, \text{ and for some } K \in \mathcal{T}_h^*\}, \\
\mathbf{M}_h^\partial(\mathbf{g}_D) &:= \{\tilde{\boldsymbol{\mu}} \in \mathbf{L}^2(\varepsilon_h^\partial) : \langle \tilde{\boldsymbol{\mu}}, \boldsymbol{\mu}^* \rangle_F = \langle \mathbf{g}_D, \boldsymbol{\mu}^* \rangle_F, \forall F \in \varepsilon_h^\partial \cap \partial\Omega_D, \text{ and } \tilde{\boldsymbol{\mu}}|_F, \boldsymbol{\mu}^*|_F \in \mathbf{P}_k(K)|_F \text{ for some } K \in \mathcal{T}_h^*\}.
\end{aligned}$$

The X-HDG scheme for problem (2.6) reads as follows: seek $(\boldsymbol{\sigma}_h, \mathbf{u}_h, \hat{\mathbf{u}}_h, \tilde{\mathbf{u}}_h) \in \mathbf{W}_h \times \mathbf{V}_h \times \mathbf{M}_h^i \times \mathbf{M}_h^\partial(\mathbf{g}_D)$ such that

$$(\mathcal{A}\boldsymbol{\sigma}_h, \mathbf{w})_{\mathcal{T}_h^*} + (\mathbf{u}_h, \nabla_h \cdot \mathbf{w})_{\mathcal{T}_h^*} - \langle \hat{\mathbf{u}}_h, \mathbf{w}\mathbf{n} \rangle_{\partial\mathcal{T}_h^* \setminus \varepsilon_h^\partial} - \langle \tilde{\mathbf{u}}_h, \mathbf{w}\mathbf{n} \rangle_{\varepsilon_h^\partial} = 0, \quad (2.7a)$$

$$-(\nabla_h \cdot \boldsymbol{\sigma}_h, \mathbf{v})_{\mathcal{T}_h^*} + \langle \tau(\mathbf{u}_h - \hat{\mathbf{u}}_h), \mathbf{v} \rangle_{\partial\mathcal{T}_h^* \setminus \varepsilon_h^\partial} + \langle \eta(\mathbf{u}_h - \tilde{\mathbf{u}}_h), \mathbf{v} \rangle_{\varepsilon_h^\partial} = (\mathbf{f}, \mathbf{v}), \quad (2.7b)$$

$$\langle \boldsymbol{\sigma}_h \mathbf{n}, \hat{\boldsymbol{\mu}} \rangle_{\partial\mathcal{T}_h^* \setminus \varepsilon_h^\partial} - \langle \tau(\mathbf{u}_h - \hat{\mathbf{u}}_h), \hat{\boldsymbol{\mu}} \rangle_{\partial\mathcal{T}_h^* \setminus \varepsilon_h^\partial} = 0, \quad (2.7c)$$

$$\langle \boldsymbol{\sigma}_h \mathbf{n}, \tilde{\boldsymbol{\mu}} \rangle_{\varepsilon_h^\partial} - \langle \eta(\mathbf{u}_h - \tilde{\mathbf{u}}_h), \tilde{\boldsymbol{\mu}} \rangle_{\varepsilon_h^\partial} = \langle \mathbf{g}_D, \tilde{\boldsymbol{\mu}} \rangle_{\varepsilon_h^\partial} \quad (2.7d)$$

for all $(\mathbf{w}, \mathbf{v}, \hat{\boldsymbol{\mu}}, \tilde{\boldsymbol{\mu}}) \in \mathbf{W}_h \times \mathbf{V}_h \times \mathbf{M}_h^i \times \mathbf{M}_h^\partial(\mathbf{0})$, and the stabilization coefficient is given by

$$\tau|_F = \eta|_F = 2\mu h_K^{-1}, \quad \forall F \in \partial K \text{ or } F = K \cap \Omega. \quad (2.8)$$

Remark 2.1. By following the same routine in the proof of Theorem 2.1, we can easily know that the scheme (2.7) admits a unique solution for $k \geq 1$.

3 A priori error estimation

This section is devoted the error analysis of the X-HDG scheme (2.2) for the linear elasticity interface problem (1.1).

3.1 Some basic results

The following lemma from [66, 67] will be used to derive an error estimate of the projection Q_r on the interface Γ (cf. Lemma 3.2).

Lemma 3.1. *There exists a positive constant h_0 depending only on the interface Γ , the shape regularity of the mesh \mathcal{T}_h , and γ in (2.1), such that for any $h \in (0, h_0]$ and $K \in \mathcal{T}_h^\Gamma$, the following estimates hold:*

$$\|v\|_{0, \Gamma_K} \lesssim h_K^{-1/2} \|v\|_{0, K \cap \Omega_i} + \|v\|_{0, K \cap \Omega_i}^{\frac{1}{2}} \|\nabla v\|_{0, K \cap \Omega_i}^{\frac{1}{2}}, \quad \forall v \in H^1(K \cap \Omega_i), \quad i = 1, 2, \quad (3.1)$$

$$\|v_h\|_{0, \Gamma_K} \lesssim h_K^{-1/2} \|v_h\|_{0, K \cap \Omega_i}, \quad \forall v_h \in P_r(K). \quad (3.2)$$

Remark 3.1. *We note that the condition $h \in (0, h_0]$ for some h_0 in this lemma is not required when Γ_K is a straight line/plane segment, and this condition is easy to satisfy when Γ_K is a curved line/surface segment.*

Based on Lemma 3.1 and standard properties of the L^2 projection operators Q_r and Q_r^b , we have the following estimates.

Lemma 3.2. *Let s be an integer with $1 \leq s \leq r + 1$. For any $K \in \mathcal{T}_h$, $h \in (0, h_0]$ and $v \in H^s((K \cap \Omega_1) \cup (K \cap \Omega_2))$, we have*

$$\begin{aligned}
\|v - Q_r v\|_{0, K} + h \|v - Q_r v\|_{1, K} &\lesssim h_K^s \|v\|_{s, K}, \\
\|v - Q_r v\|_{0, \partial K} + \|v - Q_r v\|_{0, \Gamma_K} &\lesssim h_K^{s-1/2} \|v\|_{s, K}, \\
\|v - Q_r^b v\|_{0, \partial K} &\lesssim h_K^{s-1/2} \|v\|_{s, K},
\end{aligned}$$

where the notations $\|\cdot\|_{s,K}$ and $\|\cdot\|_{0,\partial K}$ are understood respectively as $\|\cdot\|_{s,K} = \sum_{i=1}^2 \|\cdot\|_{s,K \cap \Omega_i}$ and $\|\cdot\|_{s,\partial K} = \sum_{i=1}^2 \|\cdot\|_{s,\partial K \cap \Omega_i}$ when $K \in \mathcal{T}_h^\Gamma$.

Similar to the stability results in [15, Theorem 3.4], the following continuity and coercivity conditions hold.

Lemma 3.3. *It holds the continuity condition*

$$(\mathcal{A}\sigma_h, \mathbf{w}) \leq \left\| \frac{1}{\sqrt{2\mu}} \sigma_h \right\|_{0,\mathcal{T}_h} \left\| \frac{1}{\sqrt{2\mu}} \mathbf{w} \right\|_{0,\mathcal{T}_h}, \forall \sigma_h, \mathbf{w} \in \mathbf{W}_h. \quad (3.3)$$

Moreover, it holds the coercivity condition

$$\|\mathbf{w}\|_{0,\mathcal{T}_h} \lesssim \sqrt{\mu_{max}} \left(\|\mathbf{w}\|_{0,\mathcal{A},\mathcal{T}_h} + \left\| \sqrt{\frac{h}{2\mu}} (\mathbf{w}\mathbf{n} - \hat{\mathbf{w}}\mathbf{n}) \right\|_{0,\partial\mathcal{T}_h \setminus \varepsilon_h^\Gamma} + \left\| \sqrt{\frac{h}{2\mu}} (\mathbf{w}\mathbf{n} - \tilde{\mathbf{w}}\mathbf{n}) \right\|_{*,\Gamma} \right) \quad (3.4)$$

for all $(\mathbf{w}, \hat{\mathbf{w}}, \tilde{\mathbf{w}}) \in \mathbf{W}_h \times \mathbf{L}^2(\varepsilon_h^*) \times \mathbf{L}^2(\varepsilon_h^\Gamma)$ satisfying

$$(\mathbf{w}, \nabla_h \mathbf{Q}_k \mathbf{v}) - \langle \hat{\mathbf{w}}\mathbf{n}, \mathbf{Q}_k \mathbf{v} \rangle_{\partial\mathcal{T}_h \setminus \varepsilon_h^\Gamma} - \langle \tilde{\mathbf{w}}\mathbf{n}, \mathbf{Q}_k \mathbf{v} \rangle_{*,\Gamma} = \mathbf{0}, \forall \mathbf{v} \in \mathbf{H}^1(\Omega) \text{ and } \mathbf{v}|_{\partial\Omega_D} = \mathbf{0}, \quad (3.5)$$

$$\langle \hat{\mathbf{w}}\mathbf{n}, \hat{\boldsymbol{\mu}} \rangle_{\partial\mathcal{T}_h \setminus \varepsilon_h^\Gamma} = 0, \forall \hat{\boldsymbol{\mu}} \in \mathbf{M}_h(0), \quad (3.6)$$

$$\langle \tilde{\mathbf{w}}\mathbf{n}, \tilde{\boldsymbol{\mu}} \rangle_{*,\Gamma} = 0, \forall \tilde{\boldsymbol{\mu}} \in \tilde{\mathbf{M}}_h, \quad (3.7)$$

$$\text{tr}(\mathbf{w}) \in L_0^2(\Omega), \text{ if } \Gamma_N = \emptyset, \quad (3.8)$$

where $\mu_{max} = \max_{i=1,2} \mu_i$, $\|\cdot\|_{0,\mathcal{A},\mathcal{T}_h}^2 := (\mathcal{A}, \cdot)_{0,\mathcal{T}_h}$, $\|\cdot\|_{0,\mathcal{T}_h} := (\sum_{K \in \mathcal{T}_h} \sum_{i=1}^2 \|\cdot\|_{0,K \cap \Omega_i}^2)^{\frac{1}{2}}$, $\|\cdot\|_{0,\partial\mathcal{T}_h \setminus \varepsilon_h^\Gamma} := (\sum_{F \in \partial\mathcal{T}_h \setminus \varepsilon_h^\Gamma} \sum_{i=1}^2 \|\cdot\|_{0,F \cap \Omega_i}^2)^{\frac{1}{2}}$, and $\|\cdot\|_{*,\Gamma} := \langle \cdot, \cdot \rangle_{*,\Gamma}^{\frac{1}{2}}$.

3.2 Error estimation for stress and displacement approximations

For simplicity of presentation, we define

$$\mathbf{e}_h^\sigma := \mathbf{Q}_{k-1} \boldsymbol{\sigma} - \boldsymbol{\sigma}_h, \quad \mathbf{e}_h^u := \mathbf{Q}_k \mathbf{u} - \mathbf{u}_h, \quad \mathbf{e}_h^{\hat{u}} := \mathbf{Q}_k^b \mathbf{u} - \hat{\mathbf{u}}_h, \quad \mathbf{e}_h^{\tilde{u}} := \mathbf{Q}_k^\Gamma \mathbf{u} - \tilde{\mathbf{u}}_h. \quad (3.9)$$

$$(\mathbf{Q}_k^\Gamma \mathbf{u})|_F := \begin{cases} \mathbf{Q}_k^b(\mathbf{u}|_F), & \forall F \in \varepsilon_h^\Gamma \text{ and } F \text{ is a straight segment/plane,} \\ \frac{1}{2}(\mathbf{Q}_k(\mathbf{u}|_{K \cap \Omega_1})|_F + \mathbf{Q}_k(\mathbf{u}|_{K \cap \Omega_2})|_F), & \text{otherwise.} \end{cases} \quad (3.10)$$

Then we have the following lemma on error equations.

Lemma 3.4. *For all $(\mathbf{w}, \mathbf{v}, \boldsymbol{\mu}, \tilde{\boldsymbol{\mu}}) \in \mathbf{W}_h \times \mathbf{V}_h \times \mathbf{M}_h(\mathbf{0}) \times \tilde{\mathbf{M}}_h$, it holds*

$$(\mathcal{A}\mathbf{e}_h^\sigma, \mathbf{w})_{\mathcal{T}_h} + (\mathbf{e}_h^u, \nabla_h \cdot \mathbf{w})_{\mathcal{T}_h} - \langle \mathbf{e}_h^{\hat{u}}, \mathbf{w}\mathbf{n} \rangle_{\partial\mathcal{T}_h \setminus \varepsilon_h^\Gamma} - \langle \mathbf{e}_h^{\tilde{u}}, \mathbf{w}\mathbf{n} \rangle_{*,\Gamma} = L_1(\mathbf{w}), \quad (3.11a)$$

$$-(\nabla_h \cdot \mathbf{e}_h^\sigma, \mathbf{v})_{\mathcal{T}_h} + \langle \tau(\mathbf{e}_h^u - \mathbf{e}_h^{\hat{u}}), \mathbf{v} \rangle_{\partial\mathcal{T}_h \setminus \varepsilon_h^\Gamma} + \langle \eta(\mathbf{e}_h^u - \mathbf{e}_h^{\tilde{u}}), \mathbf{v} \rangle_{*,\Gamma} = L_2(\mathbf{v}) + L_3(\mathbf{v}), \quad (3.11b)$$

$$\langle \mathbf{e}_h^\sigma \mathbf{n}, \hat{\boldsymbol{\mu}} \rangle_{\partial\mathcal{T}_h \setminus \varepsilon_h^\Gamma} - \langle \tau(\mathbf{e}_h^u - \mathbf{e}_h^{\hat{u}}), \hat{\boldsymbol{\mu}} \rangle_{\partial\mathcal{T}_h \setminus \varepsilon_h^\Gamma} = -L_2(\hat{\boldsymbol{\mu}}), \quad (3.11c)$$

$$\langle \mathbf{e}_h^\sigma \mathbf{n}, \tilde{\boldsymbol{\mu}} \rangle_{*,\Gamma} - \langle \eta(\mathbf{e}_h^u - \mathbf{e}_h^{\tilde{u}}), \tilde{\boldsymbol{\mu}} \rangle_{*,\Gamma} = -L_3(\tilde{\boldsymbol{\mu}}) \quad (3.11d)$$

for all $(\mathbf{w}, \mathbf{v}, \hat{\boldsymbol{\mu}}, \tilde{\boldsymbol{\mu}}) \in \mathbf{W}_h \times \mathbf{V}_h \times \mathbf{M}_h(\mathbf{0}) \times \tilde{\mathbf{M}}_h$, where

$$L_1(\cdot) := \langle \mathbf{u} - \mathbf{Q}_k^\Gamma \mathbf{u}, \cdot \mathbf{n} \rangle_{*,\Gamma},$$

$$L_2(\cdot) := \langle (\boldsymbol{\sigma} - \mathbf{Q}_{k-1} \boldsymbol{\sigma}) \mathbf{n}, \cdot \rangle_{\partial\mathcal{T}_h} + \langle \tau(\mathbf{Q}_k \mathbf{u} - \mathbf{Q}_k^b \mathbf{u}), \cdot \rangle_{\partial\mathcal{T}_h \setminus \varepsilon_h^\Gamma},$$

$$L_3(\cdot) := \langle (\boldsymbol{\sigma} - \mathbf{Q}_{k-1} \boldsymbol{\sigma}) \mathbf{n}, \cdot \rangle_{*,\Gamma} + \langle \eta(\mathbf{Q}_k \mathbf{u} - \mathbf{Q}_k^\Gamma \mathbf{u}), \cdot \rangle_{*,\Gamma}.$$

Proof. Let $(\boldsymbol{\sigma}, \mathbf{u})$ be the solution of (1.1). From the definition of L^2 projection and (3.10), we obtain

$$\begin{aligned} (\mathcal{A}\mathbf{Q}_{k-1}\boldsymbol{\sigma}, \mathbf{w})_{\mathcal{T}_h} + (\mathbf{Q}_k\mathbf{u}, \nabla_h \cdot \mathbf{w})_{\mathcal{T}_h} - \langle \mathbf{Q}_k^b\mathbf{u}, \mathbf{w}\mathbf{n} \rangle_{\partial\mathcal{T}_h \setminus \varepsilon_h^\Gamma} - \langle \mathbf{Q}_k^\Gamma\mathbf{u}, \mathbf{w}\mathbf{n} \rangle_{*,\Gamma} &= \langle \mathbf{u} - \mathbf{Q}_k^\Gamma\mathbf{u}, \mathbf{w}\mathbf{n} \rangle_{*,\Gamma}, \\ (\nabla_h \cdot \mathbf{Q}_{k-1}\boldsymbol{\sigma}, \mathbf{v})_{\mathcal{T}_h} - \langle \mathbf{Q}_{k-1}\boldsymbol{\sigma} - \boldsymbol{\sigma}, \mathbf{v} \rangle_{\partial\mathcal{T}_h \setminus \varepsilon_h^\Gamma} - \langle \mathbf{Q}_{k-1}\boldsymbol{\sigma} - \boldsymbol{\sigma}, \mathbf{v} \rangle_{*,\Gamma} &= \langle \mathbf{f}, \mathbf{v} \rangle, \end{aligned}$$

for any $(\mathbf{w}, \mathbf{v}) \in \mathbf{W}_h \times \mathbf{V}_h$. Subtracting (2.2a) and (2.2b) from the above two equations respectively yields (3.11a) and (3.11b). And (3.11c) and (3.11d) follow from (2.2c), (2.2d) and the relations

$$\langle \boldsymbol{\sigma}\mathbf{n}, \tilde{\boldsymbol{\mu}} \rangle_{*,\Gamma} = \langle \mathbf{g}_N^\Gamma, \tilde{\boldsymbol{\mu}} \rangle_{*,\Gamma}, \quad \langle \boldsymbol{\sigma}\mathbf{n}, \hat{\boldsymbol{\mu}} \rangle_{\partial\mathcal{T}_h \setminus \varepsilon_h^\Gamma} = \langle \mathbf{g}_N, \hat{\boldsymbol{\mu}} \rangle_{\partial\mathcal{T}_h \setminus \varepsilon_h^\Gamma}.$$

■

We introduce a semi-norm $\| \cdot \| : (\mathbf{w}, \mathbf{v}, \boldsymbol{\mu}, \tilde{\boldsymbol{\mu}}) \in \mathbf{W}_h \times \mathbf{V}_h \times \mathbf{M}_h \times \tilde{\mathbf{M}}_h \rightarrow \mathbb{R}$ with

$$\|(\mathbf{w}, \mathbf{v}, \hat{\boldsymbol{\mu}}, \tilde{\boldsymbol{\mu}})\| := (\|\mathbf{w}\|_{0,\mathcal{A},\mathcal{T}_h}^2 + \|\tau^{\frac{1}{2}}(\mathbf{v} - \hat{\boldsymbol{\mu}})\|_{\partial\mathcal{T}_h \setminus \varepsilon_h^\Gamma}^2 + \|\eta^{\frac{1}{2}}(\mathbf{v} - \tilde{\boldsymbol{\mu}})\|_{*,\Gamma}^2)^{\frac{1}{2}}. \quad (3.12)$$

Lemma 3.5. *Let $(\boldsymbol{\sigma}, \mathbf{u}) \in \mathbf{H}^k(\Omega_1 \cup \Omega_2) \times \mathbf{H}^{k+1}(\Omega_1 \cup \Omega_2)$ and $(\boldsymbol{\sigma}_h, \mathbf{u}_h, \hat{\mathbf{u}}_h, \tilde{\mathbf{u}}_h) \in \mathbf{W}_h \times \mathbf{V}_h \times \mathbf{M}_h(\mathbf{g}_D) \times \tilde{\mathbf{M}}_h$ be the solutions of the problem (1.1) and the X-HDG scheme (2.2), respectively. For any $h \in (0, h_0]$, it holds*

$$\|(\mathbf{e}_h^\sigma, \mathbf{e}_h^u, \mathbf{e}_h^{\hat{u}}, \mathbf{e}_h^{\tilde{u}})\|^2 = \sum_{i=1}^3 E_i, \quad (3.13)$$

$$\|\sqrt{2\mu}\boldsymbol{\epsilon}(\mathbf{e}_h^u)\|_{0,\mathcal{T}_h} \lesssim \begin{cases} \|(\mathbf{e}_h^\sigma, \mathbf{e}_h^u, \mathbf{e}_h^{\hat{u}}, \mathbf{e}_h^{\tilde{u}})\| + \|\frac{1}{\sqrt{2\mu}}\mathbf{e}_h^\sigma\|_{0,\mathcal{T}_h}, & \text{if interface is piecewise polygonal,} \\ \|(\mathbf{e}_h^\sigma, \mathbf{e}_h^u, \mathbf{e}_h^{\hat{u}}, \mathbf{e}_h^{\tilde{u}})\| + h^k\|\sqrt{2\mu}\mathbf{u}\|_{k+1,\mathcal{T}_h} + \|\frac{1}{\sqrt{2\mu}}\mathbf{e}_h^\sigma\|_{0,\mathcal{T}_h}, & \text{otherwise,} \end{cases} \quad (3.14)$$

where

$$\begin{aligned} E_1 &:= \langle (\mathbf{u} - \mathbf{Q}_k^\Gamma\mathbf{u}), \mathbf{e}_h^\sigma\mathbf{n} \rangle_{*,\Gamma} \\ E_2 &:= \langle (\boldsymbol{\sigma} - \mathbf{Q}_{k-1}\boldsymbol{\sigma})\mathbf{n}, \mathbf{e}_h^u - \mathbf{e}_h^{\hat{u}} \rangle_{\partial\mathcal{T}_h \setminus \varepsilon_h^\Gamma} + \langle (\boldsymbol{\sigma} - \mathbf{Q}_{k-1}\boldsymbol{\sigma})\mathbf{n}, \mathbf{e}_h^u - \mathbf{e}_h^{\tilde{u}} \rangle_{*,\Gamma}, \\ E_3 &:= \langle \tau(\mathbf{Q}_k\mathbf{u} - \mathbf{Q}_k^b\mathbf{u}), \mathbf{e}_h^u - \mathbf{e}_h^{\hat{u}} \rangle_{\partial\mathcal{T}_h \setminus \varepsilon_h^\Gamma} + \langle \eta(\mathbf{Q}_k\mathbf{u} - \mathbf{Q}_k^\Gamma\mathbf{u}), \mathbf{e}_h^u - \mathbf{e}_h^{\tilde{u}} \rangle_{*,\Gamma}. \end{aligned}$$

Proof. Taking $(\mathbf{w}, \mathbf{v}, \boldsymbol{\mu}, \tilde{\boldsymbol{\mu}}) = (\mathbf{e}_h^\sigma, \mathbf{e}_h^u, \mathbf{e}_h^{\hat{u}}, \mathbf{e}_h^{\tilde{u}})$ in the four equations in Lemma 3.11 and adding up them yield (3.13).

Then we just prove (3.14) in the case that interface is not a piecewise segment/polygon, since the piecewise segment/polygon case is easier. Taking $\mathbf{w} = 2\mu\boldsymbol{\epsilon}(\mathbf{e}_h^u)$ in (3.11a) and applying integration by parts, we obtain

$$(\mathcal{A}\mathbf{e}_h^\sigma, 2\mu\boldsymbol{\epsilon}(\mathbf{e}_h^u))_{\mathcal{T}_h} - (\nabla_h \mathbf{e}_h^u, 2\mu\boldsymbol{\epsilon}(\mathbf{e}_h^u))_{\mathcal{T}_h} + \langle \mathbf{e}_h^u - \mathbf{e}_h^{\hat{u}}, 2\mu\boldsymbol{\epsilon}(\mathbf{e}_h^u)\mathbf{n} \rangle_{\partial\mathcal{T}_h \setminus \varepsilon_h^\Gamma} + \langle \mathbf{e}_h^u - \mathbf{e}_h^{\tilde{u}}, 2\mu\boldsymbol{\epsilon}(\mathbf{e}_h^u)\mathbf{n} \rangle_{*,\Gamma} = L_1(2\mu\boldsymbol{\epsilon}(\mathbf{e}_h^u)),$$

Notice that $\boldsymbol{\epsilon}(\mathbf{e}_h^u) \in \mathbf{W}_h$ is symmetric, and we have

$$(\nabla_h \mathbf{e}_h^u, 2\mu\boldsymbol{\epsilon}(\mathbf{e}_h^u))_{\mathcal{T}_h} = \|\sqrt{2\mu}\boldsymbol{\epsilon}(\mathbf{e}_h^u)\|_{0,\mathcal{T}_h}^2.$$

From the above two relations, the Cauchy-Schwarz inequality and Lemma 3.2 it follows

$$\begin{aligned} &\|\sqrt{2\mu}\boldsymbol{\epsilon}(\mathbf{e}_h^u)\|_{0,\mathcal{T}_h}^2 \\ &= (\mathcal{A}\mathbf{e}_h^\sigma, 2\mu\boldsymbol{\epsilon}(\mathbf{e}_h^u))_{\mathcal{T}_h} + \langle \mathbf{e}_h^u - \mathbf{e}_h^{\hat{u}}, 2\mu\boldsymbol{\epsilon}(\mathbf{e}_h^u)\mathbf{n} \rangle_{\partial\mathcal{T}_h \setminus \varepsilon_h^\Gamma} + \langle \mathbf{e}_h^u - \mathbf{e}_h^{\tilde{u}}, 2\mu\boldsymbol{\epsilon}(\mathbf{e}_h^u)\mathbf{n} \rangle_{*,\Gamma} - L_1(2\mu\boldsymbol{\epsilon}(\mathbf{e}_h^u)) \\ &\lesssim \|\sqrt{2\mu}\boldsymbol{\epsilon}(\mathbf{e}_h^u)\|_{0,\mathcal{T}_h} (\|\sqrt{2\mu}\mathcal{A}\mathbf{e}_h^\sigma\|_{0,\mathcal{T}_h} + \|\tau^{\frac{1}{2}}(\mathbf{e}_h^u - \mathbf{e}_h^{\hat{u}})\|_{0,\partial\mathcal{T}_h \setminus \varepsilon_h^\Gamma} + \|\eta^{\frac{1}{2}}(\mathbf{e}_h^u - \mathbf{e}_h^{\tilde{u}})\|_{0,\partial\mathcal{T}_h \setminus \varepsilon_h^\Gamma} + \|\sqrt{\frac{2\mu}{h}}(\mathbf{u} - \mathbf{Q}_k^\Gamma\mathbf{u})\|_{*,\Gamma}). \end{aligned}$$

By the definition of operator \mathcal{A} in (1.2), we further get

$$\begin{aligned} &\|\sqrt{2\mu}\boldsymbol{\epsilon}(\mathbf{e}_h^u)\|_{0,\mathcal{T}_h} \\ &\lesssim \|\frac{1}{\sqrt{2\mu}}\mathbf{e}_h^\sigma\|_{0,\mathcal{T}_h} + \|\tau^{\frac{1}{2}}(\mathbf{e}_h^u - \mathbf{e}_h^{\hat{u}})\|_{0,\partial\mathcal{T}_h \setminus \varepsilon_h^\Gamma} + \|\eta^{\frac{1}{2}}(\mathbf{e}_h^u - \mathbf{e}_h^{\tilde{u}})\|_{0,\partial\mathcal{T}_h \setminus \varepsilon_h^\Gamma} + h^k\|\sqrt{2\mu}\mathbf{u}\|_{k+1,\mathcal{T}_h} \\ &\lesssim \|(\mathbf{e}_h^\sigma, \mathbf{e}_h^u, \mathbf{e}_h^{\hat{u}}, \mathbf{e}_h^{\tilde{u}})\| + h^k\|\sqrt{2\mu}\mathbf{u}\|_{k+1,\mathcal{T}_h} + \|\frac{1}{\sqrt{2\mu}}\mathbf{e}_h^\sigma\|_{0,\mathcal{T}_h}, \end{aligned}$$

which yields the desired estimate (3.14). ■

Set

$$\begin{aligned}\hat{e}^\sigma &:= \boldsymbol{\sigma} - \hat{\boldsymbol{\sigma}}_h, & \tilde{e}^\sigma &:= \boldsymbol{\sigma} - \tilde{\boldsymbol{\sigma}}_h, \\ (\hat{\boldsymbol{\sigma}}_h \mathbf{n})|_{F \cap \partial K} &:= \boldsymbol{\sigma}_h \mathbf{n}|_{F \cap \partial K} - \tau(\mathbf{u}_h|_{F \cap \partial K} - \hat{\mathbf{u}}_h), \quad \forall F \in \mathcal{E}_h^*, K \in \mathcal{T}_h, \\ (\tilde{\boldsymbol{\sigma}}_h \mathbf{n})|_{F \cap \tilde{\Omega}_i} &:= \boldsymbol{\sigma}_h \mathbf{n}|_{F \cap \tilde{\Omega}_i} - \eta(\mathbf{u}_h|_{F \cap \tilde{\Omega}_i} - \tilde{\mathbf{u}}_h), \quad \forall F \in \mathcal{E}_h^\Gamma, i = 1, 2.\end{aligned}$$

Then we have the following conclusion.

Lemma 3.6. *Let $(\boldsymbol{\sigma}, \mathbf{u}) \in \mathbf{H}^k(\Omega_1 \cup \Omega_2) \times \mathbf{H}^{k+1}(\Omega_1 \cup \Omega_2)$ and $(\boldsymbol{\sigma}_h, \mathbf{u}_h, \hat{\mathbf{u}}_h, \tilde{\mathbf{u}}_h) \in \mathbf{W}_h \times \mathbf{V}_h \times \mathbf{M}_h(\mathbf{g}_D) \times \tilde{\mathbf{M}}_h$ be the solutions of the problem (1.1) and the X-HDG scheme (2.2), respectively. Then it holds*

$$\|\mathbf{e}_h^\sigma\|_{0, \mathcal{T}_h} \lesssim \sqrt{\mu_{max}}(h^k \|\frac{1}{\sqrt{2\mu}} \boldsymbol{\sigma}\|_{k, \mathcal{T}_h} + h^k \|\sqrt{2\mu} \mathbf{u}\|_{k+1, \mathcal{T}_h} + \|(\mathbf{e}_h^\sigma, \mathbf{e}_h^u, \mathbf{e}_h^{\hat{u}}, \mathbf{e}_h^{\tilde{u}})\|). \quad (3.15)$$

Further more, for any $h \in (0, h_0]$,

$$\|(\mathbf{e}_h^\sigma, \mathbf{e}_h^u, \mathbf{e}_h^{\hat{u}}, \mathbf{e}_h^{\tilde{u}})\| \lesssim h^k (\sqrt{\mu_{max}} \|\mathbf{u}\|_{k+1, \Omega_1 \cup \Omega_2} + \frac{1}{\sqrt{\mu_{min}}} \|\boldsymbol{\sigma}\|_{k, \Omega_1 \cup \Omega_2}). \quad (3.16)$$

Proof. By (1.1), (2.2) and (3.9), we easily get

$$\begin{aligned}(\mathbf{e}_h^\sigma, \nabla_h \mathbf{Q}_k \mathbf{v}) - \langle \hat{\mathbf{e}}^\sigma \mathbf{n}, \mathbf{Q}_k \mathbf{v} \rangle_{\partial \mathcal{T}_h \setminus \mathcal{E}_h^\Gamma} - \langle \tilde{\mathbf{e}}^\sigma \mathbf{n}, \mathbf{Q}_k \mathbf{v} \rangle_{*, \Gamma} &= 0, \quad \forall \mathbf{v} \in \mathbf{H}^1(\Omega) \text{ and } \mathbf{v}|_{\partial \Omega_D} = \mathbf{0}, \\ \langle (\boldsymbol{\sigma} - \hat{\boldsymbol{\sigma}}_h) \mathbf{n}, \hat{\boldsymbol{\mu}} \rangle_{\partial \mathcal{T}_h \setminus \mathcal{E}_h^\Gamma} &= 0, \quad \forall \hat{\boldsymbol{\mu}} \in \mathbf{M}_h(0), \\ \langle (\boldsymbol{\sigma} - \tilde{\boldsymbol{\sigma}}_h) \mathbf{n}, \tilde{\boldsymbol{\mu}} \rangle_{*, \Gamma} &= 0, \quad \forall \tilde{\boldsymbol{\mu}} \in \tilde{\mathbf{M}}_h, \\ \text{tr}(\mathbf{e}_h^\sigma) &\in L_0^2(\Omega), \text{ if } \Gamma_N = \emptyset.\end{aligned}$$

Then from Lemma 3.3 it follows

$$\|\mathbf{e}_h^\sigma\|_{0, \mathcal{T}_h} \lesssim \sqrt{\mu_{max}} (\|\mathbf{e}_h^\sigma\|_{0, \mathcal{A}, \mathcal{T}_h} + \|\sqrt{\frac{h}{2\mu}} (\mathbf{e}_h^\sigma - \hat{\mathbf{e}}^\sigma) \mathbf{n}\|_{0, \partial \mathcal{T}_h \setminus \mathcal{E}_h^\Gamma} + \|\sqrt{\frac{h}{2\mu}} (\mathbf{e}_h^\sigma - \hat{\mathbf{e}}^\sigma) \mathbf{n}\|_{*, \Gamma}). \quad (3.17)$$

By Lemma 3.2 and the definitions of $\mathbf{e}_h^\sigma, \hat{\mathbf{e}}^\sigma, \mathbf{e}_h^u, \mathbf{e}_h^{\hat{u}}$ and $\mathbf{e}_h^{\tilde{u}}$, we have

$$\begin{aligned}& \|\sqrt{\frac{h}{2\mu}} (\mathbf{e}_h^\sigma - \hat{\mathbf{e}}^\sigma) \mathbf{n}\|_{0, \partial \mathcal{T}_h \setminus \mathcal{E}_h^\Gamma} + \|\sqrt{\frac{h}{2\mu}} (\mathbf{e}_h^\sigma - \hat{\mathbf{e}}^\sigma) \mathbf{n}\|_{*, \Gamma} \\ & \leq \|\sqrt{\frac{h}{2\mu}} (\mathbf{Q}_{k-1} \boldsymbol{\sigma} - \boldsymbol{\sigma}_h - (\boldsymbol{\sigma} - \hat{\boldsymbol{\sigma}}_h)) \mathbf{n}\|_{0, \partial \mathcal{T}_h \setminus \mathcal{E}_h^\Gamma} + \|\sqrt{\frac{h}{2\mu}} (\mathbf{Q}_{k-1} \boldsymbol{\sigma} - \boldsymbol{\sigma}_h - (\boldsymbol{\sigma} - \tilde{\boldsymbol{\sigma}}_h)) \mathbf{n}\|_{*, \Gamma} \\ & \leq h^k \|\frac{1}{\sqrt{2\mu}} \boldsymbol{\sigma}\|_{k, \mathcal{T}_h} + \|\tau^{\frac{1}{2}} (\mathbf{u}_h - \hat{\mathbf{u}}_h)\|_{0, \partial \mathcal{T}_h \setminus \mathcal{E}_h^\Gamma} + \|\eta^{\frac{1}{2}} (\mathbf{u}_h - \tilde{\mathbf{u}}_h)\|_{*, \Gamma} \\ & \leq h^k \|\frac{1}{\sqrt{2\mu}} \boldsymbol{\sigma}\|_{k, \mathcal{T}_h} + \|\tau^{\frac{1}{2}} (\mathbf{e}_h^u - \mathbf{e}_h^{\hat{u}} + \mathbf{Q}_k^b \mathbf{u} - \mathbf{Q}_k \mathbf{u})\|_{0, \partial \mathcal{T}_h \setminus \mathcal{E}_h^\Gamma} + \|\eta^{\frac{1}{2}} (\mathbf{e}_h^u - \mathbf{e}_h^{\tilde{u}} + \mathbf{Q}_k^\Gamma \mathbf{u} - \mathbf{Q}_k \mathbf{u})\|_{*, \Gamma} \\ & \leq h^k \|\frac{1}{\sqrt{2\mu}} \boldsymbol{\sigma}\|_{k, \mathcal{T}_h} + h^k \|\sqrt{2\mu} \mathbf{u}\|_{k+1, \mathcal{T}_h} + \|(\mathbf{e}_h^\sigma, \mathbf{e}_h^u, \mathbf{e}_h^{\hat{u}}, \mathbf{e}_h^{\tilde{u}})\|,\end{aligned}$$

which indicates (3.15).

The estimate (3.16) follows from Lemma 3.2 and Lemma 3.5. ■

In light of Lemma 3.5 and Lemma 3.6, we can easily derive the following optimal error estimates for the stress and displacement approximations.

Theorem 3.1. *Let $(\boldsymbol{\sigma}, \mathbf{u}) \in \mathbf{H}^k(\Omega_1 \cup \Omega_2) \times \mathbf{H}^{k+1}(\Omega_1 \cup \Omega_2)$ and $(\boldsymbol{\sigma}_h, \mathbf{u}_h, \hat{\mathbf{u}}_h, \tilde{\mathbf{u}}_h) \in \mathbf{W}_h \times \mathbf{V}_h \times \mathbf{M}_h(\mathbf{g}_D) \times \tilde{\mathbf{M}}_h$ be the solutions of the problem (1.1) and the X-HDG scheme (2.2), respectively. Then for any*

$h \in (0, h_0]$ it holds

$$\|\boldsymbol{\sigma} - \boldsymbol{\sigma}_h\|_{0, \mathcal{T}_h} \lesssim h^k (\mu_{max} \|\mathbf{u}\|_{k+1, \Omega_1 \cup \Omega_2} + \sqrt{\frac{\mu_{max}}{\mu_{min}}} \|\boldsymbol{\sigma}\|_{k, \Omega_1 \cup \Omega_2}), \quad (3.18)$$

$$\|\boldsymbol{\epsilon}(\mathbf{u}) - \boldsymbol{\epsilon}(\mathbf{u}_h)\|_{0, \mathcal{T}_h} \lesssim h^k \left(\frac{\mu_{max}}{\mu_{min}} \|\mathbf{u}\|_{k+1, \Omega_1 \cup \Omega_2} + \sqrt{\frac{\mu_{max}}{\mu_{min}^3}} \|\boldsymbol{\sigma}\|_{k, \Omega_1 \cup \Omega_2} \right). \quad (3.19)$$

Here $\mu_{min} = \min_{i=1,2} \mu_i$.

3.3 L^2 estimation for displacement approximation

To derive an L^2 error estimate for the displacement approximation by the Aubin-Nitsche's technique of duality argument, we need to introduce an auxiliary problem:

$$\mathcal{A}\Phi - \boldsymbol{\epsilon}(\phi) = \mathbf{0}, \quad \text{in } \Omega_1 \cup \Omega_2 \quad (3.20a)$$

$$\nabla \cdot \Phi = \mathbf{e}_h^u, \quad \text{in } \Omega_1 \cup \Omega_2 \quad (3.20b)$$

$$\phi = \mathbf{0}, \quad \text{on } \partial\Omega_D \quad (3.20c)$$

$$\Phi \mathbf{n} = \mathbf{0}, \quad \text{on } \partial\Omega_N \quad (3.20d)$$

$$[[\phi]] = \mathbf{0}, \quad [[\Phi \mathbf{n}]] = \mathbf{0}, \quad \text{on } \Gamma, \quad (3.20e)$$

where $\mathbf{e}_h^u = \mathbf{Q}_k \mathbf{u} - \mathbf{u}_h$. In addition, we assume that the following regularity estimate holds:

$$\|\Phi\|_{H^1(\Omega_1 \cup \Omega_2)} + \|\mu\phi\|_{H^2(\Omega_1 \cup \Omega_2)} \lesssim \|\mathbf{e}_h^u\|_{0, \mathcal{T}_h}. \quad (3.21)$$

Theorem 3.2. *Let $(\boldsymbol{\sigma}, \mathbf{u}) \in \mathbf{H}^k(\Omega_1 \cup \Omega_2) \times \mathbf{H}^{k+1}(\Omega_1 \cup \Omega_2)$ and $(\boldsymbol{\sigma}_h, \mathbf{u}_h, \hat{\mathbf{u}}_h, \tilde{\mathbf{u}}_h) \in \mathbf{W}_h \times \mathbf{V}_h \times \mathbf{M}_h(\mathbf{g}_D) \times \tilde{\mathbf{M}}_h$ be the solutions of the problem (1.1) and the X-HDG scheme (2.2), respectively. Then for any $h \in (0, h_0]$ it holds the error estimate*

$$\|\mathbf{u} - \mathbf{u}_h\|_{0, \mathcal{T}_h} \lesssim h^{k+1} \left(\frac{\mu_{max}}{\mu_{min}} \|\mathbf{u}\|_{k+1, \Omega_1 \cup \Omega_2} + \sqrt{\frac{\mu_{max}}{\mu_{min}^3}} \|\boldsymbol{\sigma}\|_{k, \Omega_1 \cup \Omega_2} \right). \quad (3.22)$$

Proof. Testing the equations (3.20b) by \mathbf{e}_h^u and using the projection properties and integration by parts, we have

$$\begin{aligned} \|\mathbf{e}_h^u\|_{0, \mathcal{T}_h}^2 &= (\nabla_h \cdot \Phi, \mathbf{e}_h^u)_{\mathcal{T}_h} \\ &= (\nabla_h \cdot \mathbf{Q}_{k-1} \Phi, \mathbf{e}_h^u)_{\mathcal{T}_h} + \langle (\Phi - \mathbf{Q}_{k-1} \Phi) \mathbf{n}, \mathbf{e}_h^u \rangle_{\partial\mathcal{T}_h \setminus \varepsilon_h^\Gamma} + \langle (\Phi - \mathbf{Q}_{k-1} \Phi) \mathbf{n}, \mathbf{e}_h^u \rangle_{*, \Gamma}, \end{aligned}$$

which, together with the fact that $[[\Phi \mathbf{n}]] = \mathbf{0}$ on Γ and the error equation (3.11a), implies

$$\begin{aligned} \|\mathbf{e}_h^u\|_{0, \mathcal{T}_h}^2 &= L_1(\mathbf{Q}_{k-1} \Phi) - (\mathcal{A} \mathbf{e}_h^\sigma, \mathbf{Q}_{k-1} \Phi)_{\mathcal{T}_h} + \langle (\Phi - \mathbf{Q}_{k-1} \Phi) \mathbf{n}, \mathbf{e}_h^u - \mathbf{e}_h^{\hat{u}} \rangle_{\partial\mathcal{T}_h \setminus \varepsilon_h^\Gamma} \\ &\quad + \langle (\Phi - \mathbf{Q}_{k-1} \Phi) \mathbf{n}, \mathbf{e}_h^u - \mathbf{e}_h^{\hat{u}} \rangle_{*, \Gamma}. \end{aligned} \quad (3.23)$$

Taking $(\mathbf{v}, \hat{\boldsymbol{\mu}}, \tilde{\boldsymbol{\mu}}) = (\mathbf{Q}_k \phi, \mathbf{Q}_k^b \phi, \mathbf{Q}_k^\Gamma \phi)$ in (3.11b)-(3.11d) yields that

$$\begin{aligned} -(\nabla_h \cdot \mathbf{e}_h^\sigma, \mathbf{Q}_k \phi)_{\mathcal{T}_h} + \langle \tau(\mathbf{e}_h^u - \mathbf{e}_h^{\hat{u}}), \mathbf{Q}_k \phi \rangle_{\partial\mathcal{T}_h \setminus \varepsilon_h^\Gamma} + \langle \eta(\mathbf{e}_h^u - \mathbf{e}_h^{\hat{u}}), \mathbf{Q}_k \phi \rangle_{*, \Gamma} &= \sum_{i=2}^3 L_i(\mathbf{Q}_k \phi), \\ \langle \mathbf{e}_h^\sigma \mathbf{n}, \mathbf{Q}_k^b \phi \rangle_{\partial\mathcal{T}_h \setminus \varepsilon_h^\Gamma} - \langle \tau(\mathbf{e}_h^u - \mathbf{e}_h^{\hat{u}}), \mathbf{Q}_k^b \phi \rangle_{\partial\mathcal{T}_h \setminus \varepsilon_h^\Gamma} &= -L_2(\mathbf{Q}_k^b \phi), \\ \langle \mathbf{e}_h^\sigma \mathbf{n}, \mathbf{Q}_k^\Gamma \phi \rangle_{*, \Gamma} - \langle \eta(\mathbf{e}_h^u - \mathbf{e}_h^{\hat{u}}), \mathbf{Q}_k^\Gamma \phi \rangle_{*, \Gamma} &= -L_3(\mathbf{Q}_k^\Gamma \phi). \end{aligned}$$

These relations plus (3.20) lead to

$$\begin{aligned} &(\mathcal{A}\Phi, \mathbf{e}_h^\sigma)_{\mathcal{T}_h} \\ &= -(\phi, \nabla_h \cdot \mathbf{e}_h^\sigma)_{\mathcal{T}_h} + \langle \phi, \mathbf{e}_h^\sigma \mathbf{n} \rangle_{\partial\mathcal{T}_h \setminus \varepsilon_h^\Gamma} + \langle \phi, \mathbf{e}_h^\sigma \mathbf{n} \rangle_{*, \Gamma} \\ &= -(\mathbf{Q}_k \phi, \nabla_h \cdot \mathbf{e}_h^\sigma)_{\mathcal{T}_h} + \langle \mathbf{Q}_k^b \phi, \mathbf{e}_h^\sigma \mathbf{n} \rangle_{\partial\mathcal{T}_h \setminus \varepsilon_h^\Gamma} + \langle \mathbf{Q}_k^\Gamma \phi, \mathbf{e}_h^\sigma \mathbf{n} \rangle_{*, \Gamma} + \langle \phi - \mathbf{Q}_k^\Gamma \phi, \mathbf{e}_h^\sigma \mathbf{n} \rangle_{*, \Gamma} \\ &= L_2(\mathbf{Q}_k \phi - \mathbf{Q}_k^b \phi) + L_3(\mathbf{Q}_k \phi - \mathbf{Q}_k^\Gamma \phi) + \langle \tau(\mathbf{e}_h^u - \mathbf{e}_h^{\hat{u}}), \mathbf{Q}_k^b \phi - \mathbf{Q}_k \phi \rangle_{\partial\mathcal{T}_h \setminus \varepsilon_h^\Gamma} + \langle \eta(\mathbf{e}_h^u - \mathbf{e}_h^{\hat{u}}), \mathbf{Q}_k^\Gamma \phi - \mathbf{Q}_k \phi \rangle_{*, \Gamma} \\ &\quad + \langle \phi - \mathbf{Q}_k^\Gamma \phi, \mathbf{e}_h^\sigma \mathbf{n} \rangle_{*, \Gamma}. \end{aligned}$$

By (3.23) we further get

$$\|e_h^u\|_{0,\mathcal{T}_h}^2 = \sum_{j=1}^4 I_j + (\mathbf{Q}_{k-1}\Phi - \Phi, \mathcal{A}e_h^\sigma)_{\mathcal{T}_h},$$

where

$$\begin{aligned} I_1 &:= \langle (\mathbf{Q}_{k-1}\Phi - \Phi)\mathbf{n}, e_h^u - e_h^{\hat{u}} \rangle_{\partial\mathcal{T}_h \setminus \varepsilon_h^\Gamma} + \langle (\mathbf{Q}_{k-1}\Phi - \Phi)\mathbf{n}, e_h^u - e_h^{\hat{u}} \rangle_{*,\Gamma}, \\ I_2 &:= L_2(\mathbf{Q}_k\phi - \mathbf{Q}_k^b\phi) + L_3(\mathbf{Q}_k\phi - \mathbf{Q}_k^\Gamma\phi), \\ I_3 &:= \langle \tau(e_h^u - e_h^{\hat{u}}), \mathbf{Q}_k^b\phi - \mathbf{Q}_k\phi \rangle_{\partial\mathcal{T}_h \setminus \varepsilon_h^\Gamma} + \langle \eta(e_h^u - e_h^{\hat{u}}), \mathbf{Q}_k^\Gamma\phi - \mathbf{Q}_k\phi \rangle_{*,\Gamma}, \\ I_4 &:= \langle \phi - \mathbf{Q}_k^\Gamma\phi, e_h^\sigma \mathbf{n} \rangle_{*,\Gamma} + L_1(\mathbf{Q}_{k-1}\Phi). \end{aligned}$$

In light of the Cauchy-Schwarz inequality, Lemma 3.2 and the definition of operator \mathcal{A} in (1.2), we obtain

$$\begin{aligned} (\mathbf{Q}_{k-1}\Phi - \Phi, \mathcal{A}e_h^\sigma)_{\mathcal{T}_h} &\leq \| \mathcal{A}e_h^\sigma \|_{0,\mathcal{T}_h} \| \mathbf{Q}_{k-1}\Phi - \Phi \|_{0,\mathcal{T}_h} \\ &\lesssim h \| \mu^{-1}e_h^\sigma \|_{0,\mathcal{T}_h} \| \Phi \|_{1,\Omega_1 \cup \Omega_2}. \end{aligned}$$

From the definition of $\| \cdot \|$ it follows

$$\begin{aligned} I_1 &\leq \| (\mathbf{Q}_{k-1}\Phi - \Phi) \|_{\partial\mathcal{T}_h \setminus \varepsilon_h^\Gamma} \| \tau^{-\frac{1}{2}} \tau^{\frac{1}{2}} (e_h^u - e_h^{\hat{u}}) \|_{\partial\mathcal{T}_h \setminus \varepsilon_h^\Gamma} + \| (\mathbf{Q}_{k-1}\Phi - \Phi) \|_{*,\Gamma} \| \eta^{-\frac{1}{2}} \eta^{\frac{1}{2}} (e_h^u - e_h^{\hat{u}}) \|_{*,\Gamma} \\ &\lesssim h \| \Phi \|_{1,\Omega_1 \cup \Omega_2} \| \mu^{-\frac{1}{2}} (e_h^\sigma, e_h^u, e_h^{\hat{u}}, e_h^{\tilde{u}}) \| . \end{aligned}$$

Similarly, we can obtain the estimates of I_2, I_3 , i.e.

$$\begin{aligned} I_2 &\leq h^{k+1} \| \mu\phi \|_{2,\Omega_1 \cup \Omega_2} (\| \mu^{-1}\sigma \|_{k,\Omega_1 \cup \Omega_2} + \| \mathbf{u} \|_{k+1,\Omega_1 \cup \Omega_2}), \\ I_3 &\leq h \| \mu\phi \|_{2,\Omega_1 \cup \Omega_2} \| \mu^{-\frac{1}{2}} (e_h^\sigma, e_h^u, e_h^{\hat{u}}, e_h^{\tilde{u}}) \| . \end{aligned}$$

It remains to estimate I_4 . Due to the fact that $\mathbf{u}, \mathbf{Q}_k^\Gamma \mathbf{u}$ and Φ are all single-valued on $F \in \varepsilon_h^*$, we have

$$\begin{aligned} I_4 &= \langle \phi - \mathbf{Q}_k^\Gamma\phi, e_h^\sigma \mathbf{n} \rangle_{*,\Gamma} + \langle \mathbf{u} - \mathbf{Q}_k^\Gamma \mathbf{u}, \mathbf{Q}_{k-1}\Phi \mathbf{n} \rangle_{*,\Gamma} \\ &= \langle \phi - \mathbf{Q}_k^\Gamma\phi, e_h^\sigma \mathbf{n} \rangle_{*,\Gamma} + \langle \mathbf{u} - \mathbf{Q}_k^\Gamma \mathbf{u}, (\mathbf{Q}_{k-1}\Phi - \Phi)\mathbf{n} \rangle_{*,\Gamma} \\ &\lesssim h \| \mu^{-1}e_h^\sigma \|_{0,\mathcal{T}_h} \| \mu\phi \|_{2,\Omega_1 \cup \Omega_2} + h^{k+1} \| \mathbf{u} \|_{k+1,\Omega_1 \cup \Omega_2} \| \Phi \|_{1,\Omega_1 \cup \Omega_2}. \end{aligned}$$

The above estimates, together with the regularity assumption (3.21) and Theorem 3.1, imply the desired estimate (3.22). \blacksquare

Remark 3.2. *By following the same routines as in the analysis of the interface-unfitted scheme (2.2), it is easy to see that Theorem 3.1 and Theorem 3.2 still hold for the boundary-unfitted scheme (2.7) in either of the following two cases:*

- (i) *The Dirichlet boundary condition in (2.5) is homogeneous, i.e. $\llbracket \mathbf{u} \rrbracket = 0$ on $\partial\Omega_D$;*
- (ii) *The domain Ω is a convex polygon.*

4 Numerical experiments

In this section, we shall provide several numerical examples to verify the performance of the proposed interface/boundary-unfitted X-HDG method.

Example 4.1. *A plane strain test with a circular interface.*

This example is a plane strain test. In (1.1) we set (cf. Figure 4)

$$\Omega = [0, 1]^2, \quad \Omega_2 = (x, y) : (x - \frac{1}{2})^2 + (y - \frac{1}{2})^2 < \frac{3}{64}, \quad \text{and } \Omega_1 = \Omega \setminus \bar{\Omega}_2.$$

The exact solution $(\mathbf{u}, \boldsymbol{\sigma})$ in $\Omega_1 \cup \Omega_2$ is given by

$$\mathbf{u}(x, y) = \begin{pmatrix} -x^2(x-1)^2y(y-1)(2y-1) \\ y^2(y-1)^2x(x-1)(2x-1) \end{pmatrix}, \quad \boldsymbol{\sigma}(x, y) = 2\mu\boldsymbol{\epsilon}(\mathbf{u}) + \lambda\text{div } \mathbf{u} \mathbf{I},$$

where the Lamé coefficients $\mu = \frac{E}{2(1+\nu)}$, $\lambda = \frac{E\nu}{(1+\nu)(1-2\nu)}$, with the Young's modulus $E|_{\Omega_1 \cup \Omega_2} = 3$, the Poisson ratio $\nu|_{\Omega_1} = 0.4$ and $\nu|_{\Omega_2} = 0.4, 0.49, 0.4999, 0.499999$. We note that the material tends to incompressible as $\nu \rightarrow 0.5$ (or $\lambda \rightarrow \infty$). The force term, boundary conditions and interface conditions can be derived explicitly.

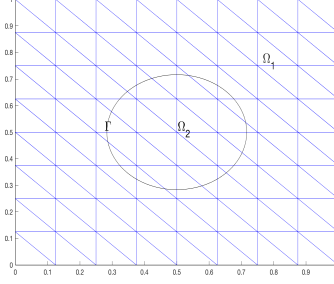


Figure 4: The domain with a circular interface: 8×8 mesh

We use $N \times N$ uniform triangular meshes for the computation. Errors of displacement and stress approximations with $k = 1, 2$ are shown in Table 1. We can see that our X-HDG method (2.2) yields $(k+1)$ -th and k -th orders of convergence for $\|\mathbf{u} - \mathbf{u}_h\|_0$ and $\|\boldsymbol{\sigma} - \boldsymbol{\sigma}_h\|_0$, respectively, which are uniform as ν tends to 0.5. These results are conformable to Theorems 3.2 and 3.1.

$\nu _{\Omega_2}$	mesh	$k = 1$				$k = 2$			
		$\frac{\ \mathbf{u} - \mathbf{u}_h\ _0}{\ \mathbf{u}\ _0}$		$\frac{\ \boldsymbol{\sigma} - \boldsymbol{\sigma}_h\ _0}{\ \boldsymbol{\sigma}\ _0}$		$\frac{\ \mathbf{u} - \mathbf{u}_h\ _0}{\ \mathbf{u}\ _0}$		$\frac{\ \boldsymbol{\sigma} - \boldsymbol{\sigma}_h\ _0}{\ \boldsymbol{\sigma}\ _0}$	
		error	order	error	order	error	order	error	order
0.4	8×8	1.3656E-01	–	3.0139E-01	–	8.6182E-03	–	4.5657E-02	–
	16×16	3.7733E-02	1.86	1.4693E-01	1.04	1.3317E-03	2.69	1.1478E-02	1.99
	32×32	9.8295E-03	1.94	7.2247E-02	1.02	1.8939E-04	2.81	2.7901E-03	2.04
	64×64	2.4915E-03	1.98	3.5934E-02	1.01	2.5407E-05	2.90	6.7861E-04	2.04
0.49	8×8	1.3343E-01	–	3.0096E-01	–	8.6171E-03	–	4.5613E-02	–
	16×16	3.6398E-02	1.87	1.4674E-01	1.04	1.3315E-03	2.69	1.1463E-02	1.99
	32×32	9.4020E-03	1.95	7.2150E-02	1.02	1.8936E-04	2.81	2.7857E-03	2.04
	64×64	2.2876E-03	2.04	3.5885E-02	1.01	2.5404E-05	2.90	6.7738E-04	2.04
0.4999	8×8	1.3312E-01	–	3.0093E-01	–	8.6171E-03	–	4.5609E-02	–
	16×16	3.6268E-02	1.88	1.4673E-01	1.04	1.3315E-03	2.69	1.1461E-02	1.99
	32×32	9.3616E-03	1.95	7.2142E-02	1.02	1.8936E-04	2.81	2.7852E-03	2.04
	64×64	2.2709E-03	2.04	3.5881E-02	1.01	2.5404E-05	2.90	6.7726E-04	2.04
0.499999	8×8	1.3311E-01	–	3.0093E-01	–	8.6171E-03	–	4.5609E-02	–
	16×16	3.6266E-02	1.88	1.4673E-01	1.04	1.3315E-03	2.69	1.1461E-02	1.99
	32×32	9.3612E-03	1.95	7.2142E-02	1.02	1.8936E-04	2.81	2.7852E-03	2.04
	64×64	2.2709E-03	2.04	3.5881E-02	1.01	2.5404E-05	2.90	6.7726E-04	2.04

Table 1: History of convergence: Example 4.1

Remark 4.1. We note that in implementation of the scheme (2.2) on very refined meshes one may need some special handling of the approximation space $\tilde{\mathbf{M}}_h = \{\tilde{\boldsymbol{\mu}} \in \mathbf{L}^2(F) : \tilde{\boldsymbol{\mu}}|_F \in \mathbf{P}_k(K)|_F, \forall F \in \mathcal{E}_h^\Gamma\}$. Taking the circular interface in 2 – dimension as an example, when the mesh size h becomes small enough, $F \in \mathcal{E}_h^\Gamma$ will be close to a line segment. In this situation, the coordinates x and y on F are approximately linearly-dependent. Thus, the direct use of $\tilde{\mathbf{M}}_h$ may lead to a very large condition number of the resultant stiffness matrix. In this situation, one can replace $\tilde{\mathbf{M}}_h$ with

$$\tilde{\mathbf{M}}_h^{*1} = \{\tilde{\boldsymbol{\mu}} \in \mathbf{L}^2(F) : \tilde{\boldsymbol{\mu}}|_F \in \text{span}\{1, x, \dots, x^k\}, \forall F \in \mathcal{E}_h^\Gamma\}$$

or

$$\tilde{\mathbf{M}}_h^{*2} = \{\tilde{\boldsymbol{\mu}} \in \mathbf{L}^2(F) : \tilde{\boldsymbol{\mu}}|_F \in \text{span}\{1, y, \dots, y^k\}, \forall F \in \varepsilon_h^\Gamma\}$$

according to the average slope of F . Numerical tests indicate that such a modification does not affect the accuracy of the scheme.

Example 4.2. A plane strain test on a circular domain: boundary-unfitted meshes.

This example is to test the performance of the X-HDG scheme (2.7) with boundary-unfitted meshes (cf. Figure 5). In (2.5) we set

$$\Omega = \{(x, y) : (x - \frac{1}{2})^2 + (y - \frac{1}{2})^2 < \frac{3}{16}\}.$$

And the exact solution $(\mathbf{u}, \boldsymbol{\sigma})$ has the same form as in Example 4.1, i.e.

$$\mathbf{u}(x, y) = \begin{pmatrix} -x^2(x-1)^2y(y-1)(2y-1) \\ y^2(y-1)^2x(x-1)(2x-1) \end{pmatrix}, \quad \boldsymbol{\sigma}(x, y) = \frac{E}{1+\nu}\boldsymbol{\epsilon}(\mathbf{u}) + \frac{E\nu}{(1+\nu)(1-2\nu)}\text{div } \mathbf{u} \mathbf{I},$$

where the Young's modulus $E = 3$, and the Poisson ratio $\nu = 0.49, 0.4999, 0.499999$.

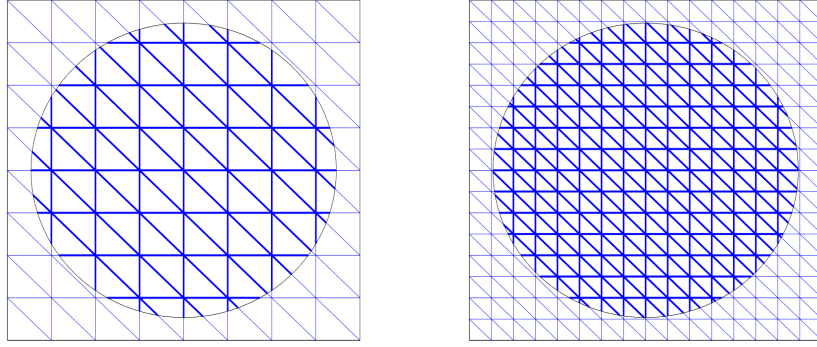


Figure 5: The geometry of domain in Example 4.2: 8×8 (left) and 16×16 (right) meshes

In (2.7) we take $\mathbb{B} = [0, 1]^2$, and use $N \times N$ uniform triangular meshes. Numerical results listed in Table 2 for $k = 1$ and $k = 2$ show that our X-HDG method (2.7) yields $(k + 1)$ -th and k -th orders of uniform convergence for $\|\mathbf{u} - \mathbf{u}_h\|_0$ and $\|\boldsymbol{\sigma} - \boldsymbol{\sigma}_h\|_0$, respectively.

ν	mesh	$k = 1$				$k = 2$			
		$\frac{\ \mathbf{u} - \mathbf{u}_h\ _0}{\ \mathbf{u}\ _0}$		$\frac{\ \boldsymbol{\sigma} - \boldsymbol{\sigma}_h\ _0}{\ \boldsymbol{\sigma}\ _0}$		$\frac{\ \mathbf{u} - \mathbf{u}_h\ _0}{\ \mathbf{u}\ _0}$		$\frac{\ \boldsymbol{\sigma} - \boldsymbol{\sigma}_h\ _0}{\ \boldsymbol{\sigma}\ _0}$	
		error	order	error	order	error	order	error	order
0.49	8×8	5.3684E-02	–	2.4740E-01	–	4.8695E-03	–	3.1598E-02	–
	16×16	1.4048E-02	1.93	1.2945E-01	0.93	6.7638E-04	2.85	8.4985E-03	1.89
	32×32	3.5215E-03	2.00	6.4187E-02	1.01	9.2824E-05	2.87	2.1532E-03	1.98
	64×64	8.8990E-04	1.98	3.1914E-02	1.01	1.2318E-05	2.91	5.3899E-04	2.00
0.4999	8×8	5.3551E-02	–	2.4783E-01	–	4.8595E-03	–	3.1711E-02	–
	16×16	1.3991E-02	1.94	1.2974E-01	0.93	6.7533E-04	2.85	8.5228E-03	1.90
	32×32	3.5087E-03	2.00	6.4289E-02	1.01	9.2709E-05	2.86	2.1575E-03	1.98
	64×64	8.8752E-04	1.98	3.1944E-02	1.01	1.2305E-05	2.91	5.3966E-04	2.00
0.499999	8×8	5.3549E-02	–	2.4784E-01	–	4.8594E-03	–	3.1713E-02	–
	16×16	1.3991E-02	1.94	1.2975E-01	0.93	6.7532E-04	2.85	8.5231E-03	1.90
	32×32	3.5085E-03	2.00	6.4290E-02	1.01	9.3270E-05	2.86	2.1670E-03	1.98
	64×64	8.8749E-04	1.98	3.1944E-02	1.01	1.2305E-05	2.92	5.3967E-04	2.01

Table 2: History of convergence: Example 4.2

Example 4.3. A test on a non-convex domain: inner-boundary-unfitted meshes.

This example is also used to test the performance of the X-HDG scheme (2.7) with boundary-unfitted meshes (cf. Figure 6). Set

$$\Omega = [0, 1]^2 \setminus \{(x, y) : (x - \frac{1}{2})^2 + (y - \frac{1}{2})^2 < \frac{3}{64}\}.$$

The exact solution $(\mathbf{u}, \boldsymbol{\sigma})$ of problem (2.5) is given by

$$\mathbf{u}(x, y) = \begin{pmatrix} y^4 \\ x^4 \end{pmatrix}, \quad \boldsymbol{\sigma}(x, y) = 2\mu\boldsymbol{\epsilon}(\mathbf{u}) + \lambda \operatorname{div} \mathbf{u} \mathbf{I},$$

where the Lamé coefficients $\mu = 1, \lambda = 1, 10^9$.

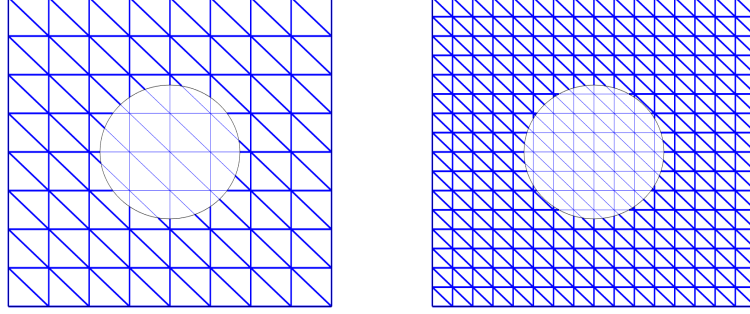


Figure 6: The geometry of domain in Example 4.3: 8×8 (left) and 16×16 (right) meshes

In (2.7) we take $\mathbb{B} = [0, 1]^2$, and use $N \times N$ uniform triangular meshes. Numerical results in Table 3 for $k = 1$ and $k = 2$ demonstrate that the proposed X-HDG method is of $(k + 1)$ -th and k -th orders of convergence for $\|\mathbf{u} - \mathbf{u}_h\|_0$ and $\|\boldsymbol{\sigma} - \boldsymbol{\sigma}_h\|_0$, respectively.

k	mesh	$\lambda = 1$				$\lambda = 10^9$			
		$\frac{\ \mathbf{u} - \mathbf{u}_h\ _0}{\ \mathbf{u}\ _0}$		$\frac{\ \boldsymbol{\sigma} - \boldsymbol{\sigma}_h\ _0}{\ \boldsymbol{\sigma}\ _0}$		$\frac{\ \mathbf{u} - \mathbf{u}_h\ _0}{\ \mathbf{u}\ _0}$		$\frac{\ \boldsymbol{\sigma} - \boldsymbol{\sigma}_h\ _0}{\ \boldsymbol{\sigma}\ _0}$	
		error	order	error	order	error	order	error	order
1	8×8	2.3323E-02	–	8.7293E-02	–	1.7339E-02	–	1.2011E-01	–
	16×16	6.2669E-03	1.90	4.1513E-02	1.07	5.1284E-03	1.76	5.3700E-02	1.16
	32×32	1.6009E-03	1.97	2.0172E-02	1.04	1.4018E-03	1.87	2.2952E-02	1.23
	64×64	4.0156E-04	2.00	9.9689E-03	1.02	3.6201E-04	1.95	1.0511E-02	1.13
2	8×8	1.5152E-03	–	4.9384E-03	–	1.4237E-03	–	5.8621E-03	–
	16×16	2.2757E-04	2.74	1.1363E-03	2.12	2.2009E-04	2.69	1.2826E-03	2.19
	32×32	3.0812E-05	2.88	2.6608E-04	2.09	3.0196E-05	2.87	2.8741E-04	2.16
	64×64	3.9847E-06	2.95	6.3934E-05	2.06	3.9278E-06	2.94	6.7190E-05	2.10

Table 3: History of convergence: Example 4.3

Example 4.4. A plane stress test in crack-tip domain.

This example is a near crack-tip plane stress problem [5]. In (2.5) we take

$$\Omega = [0, 1]^2 \setminus \{(x, y_c) : 0 \leq x \leq x_c\}$$

with the crack $\partial\Omega_N = \{(x, y_c) : 0 \leq x \leq x_c\}$ (cf. Figure 7), and $\partial\Omega_D = \partial\Omega \setminus \partial\Omega_N$, where $(x_c, y_c) = (\frac{1}{2}, \frac{1}{2})$ is the crack tip. The Lamé coefficients $\mu = \frac{E}{2(1+\nu)}$ and $\lambda = \frac{E\nu}{(1+\nu)(1-\nu)}$ with $\nu = 1/3, E = 8/3$. The exact solution $(\mathbf{u}, \boldsymbol{\sigma})$ is given by

$$\mathbf{u}(x, y) = \begin{pmatrix} \frac{K_I}{2\mu} \sqrt{\frac{r}{2\pi}} \cos(\frac{\theta}{2}) [\kappa - 1 + 2\sin^2(\frac{\theta}{2})] \\ \frac{K_I}{2\mu} \sqrt{\frac{r}{2\pi}} \sin(\frac{\theta}{2}) [\kappa + 1 - 2\cos^2(\frac{\theta}{2})] \end{pmatrix},$$

$$\boldsymbol{\sigma}(x, y) = \begin{pmatrix} \frac{K_I}{\sqrt{2\pi r}} \cos(\frac{\theta}{2}) [1 - \sin(\frac{\theta}{2}) \sin(\frac{3\theta}{2})], & \frac{K_I}{\sqrt{2\pi r}} \cos(\frac{\theta}{2}) \sin(\frac{\theta}{2}) \cos(\frac{3\theta}{2}) \\ \frac{K_I}{\sqrt{2\pi r}} \cos(\frac{\theta}{2}) \sin(\frac{\theta}{2}) \cos(\frac{3\theta}{2}), & \frac{K_I}{\sqrt{2\pi r}} \cos(\frac{\theta}{2}) [1 + \sin(\frac{\theta}{2}) \sin(\frac{3\theta}{2})] \end{pmatrix},$$

where r is the distance from the crack tip, $\theta = \arctan 2(y - y_c, x - x_c)$, $\kappa = \frac{3-\nu}{1+\nu}$, and the stress intensity factor (SIF) $K_I = \sqrt{\frac{\pi}{2}}$. We note that the boundary condition along the line crack is a homogeneous Neumann condition, i.e. $\boldsymbol{\sigma} \mathbf{n}|_{\partial\Omega_N} = 0$, and that $\mathbf{u} \notin \mathbf{H}^{3/2}(\Omega)$ but $\mathbf{u} \in \mathbf{H}^{3/2-\epsilon}(\Omega)$ for any $\epsilon > 0$.

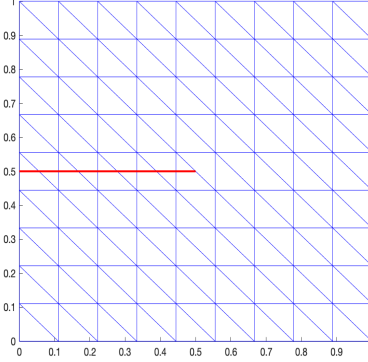


Figure 7: The crack domain in Example 4.4: 9×9 mesh

In the X-HDG scheme (2.7) we take $\mathbb{B} = [0, 1]^2$, and use $N \times N$ uniform triangular meshes. Due to the low regularity of the exact solution, we only consider the lowest order case of the scheme, i.e. $k = 1$. From the numerical results in Table 4, we can see that the convergence rate is 0.5 for the stress error $\|\boldsymbol{\sigma} - \boldsymbol{\sigma}_h\|_0$, which is as same as that in [5], and that the convergence rate is 1 for the displacement error $\|\mathbf{u} - \mathbf{u}_h\|_0$. The second component of the displacement approximation \mathbf{u}_h at 129×129 mesh is also plotted in Figure 8.

k	mesh	$\frac{\ \mathbf{u} - \mathbf{u}_h\ _0}{\ \mathbf{u}\ _0}$		$\frac{\ \boldsymbol{\sigma} - \boldsymbol{\sigma}_h\ _0}{\ \boldsymbol{\sigma}\ _0}$	
		error	order	error	order
1	9×9	3.5241E-02	—	2.5316E-01	—
	17×17	1.9991E-02	0.89	1.8320E-01	0.51
	33×33	1.0712E-02	0.94	1.3107E-01	0.50
	65×65	5.5568E-03	0.97	9.3236E-02	0.50
	129×129	2.8322E-03	0.98	6.6125E-02	0.50

Table 4: History of convergence for Example 4.4

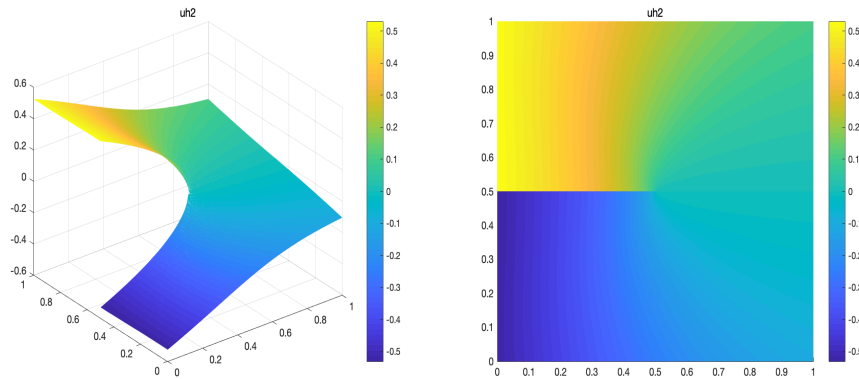


Figure 8: The second component of displacement approximation in Example 4.4: 129×129 mesh

5 Conclusions

In this paper, we have proposed and analyzed an arbitrary order interface/boundary-unfitted eXtended hybridizable discontinuous Galerkin method for linear elasticity interface problems. This X-HDG method is of optimal convergence uniformly in the Lamé constant λ . Numerical experiments have demonstrated the performance and robustness of method.

References

- [1] S. Adjerid, N. Chaabane, and T. Lin. An immersed discontinuous finite element method for Stokes interface problems. *Computer Methods in Applied Mechanics & Engineering*, 293:170–190, 2015. [3](#)
- [2] I. Babuška. The finite element method for elliptic equations with discontinuous coefficients. *Computing*, 5(3):207–213, 1970. [2](#)
- [3] I. Babuška and U. Banerjee. Stable generalized finite element method (SGFEM). *Computer Methods in Applied Mechanics & Engineering*, 201(1):91–111, 2011. [2](#)
- [4] I. Babuška, G. Caloz, and J. E. Osborn. Special finite element methods for a class of second order elliptic problems with rough coefficients. *SIAM Journal on Numerical Analysis*, 31(4):945–981, 1994. [2](#)
- [5] E. Barbieri, N. Petrinic, M. Meo, and V. L. Tagarielli. A new weight-function enrichment in meshless methods for multiple cracks in linear elasticity. *International Journal for Numerical Methods in Engineering*, 90(2):177–195, 2012. [15](#), [16](#)
- [6] J. W. Barrett and C. M. Elliott. Fitted and unfitted finite element methods for elliptic equations with smooth interfaces. *IMA Journal of Numerical Analysis*, 7(3):283–300, 1987. [2](#)
- [7] R. Becker, E. Burman, and P. Hansbo. A Nitsche extended finite element method for incompressible elasticity with discontinuous modulus of elasticity. *Computer Methods in Applied Mechanics & Engineering*, 198(41):3352–3360, 2009. [2](#), [3](#)
- [8] T. Belytschko, R. Gracie, and G. Ventura. A review of extended/generalized finite element methods for material modeling. *Modelling and Simulation in Materials Science and Engineering*, 17(4):043001, 2009. [2](#)
- [9] O. Bodart, V. Cayol, S. Court, and J. Koko. XFEM-based fictitious domain method for linear elasticity model with crack. *SIAM Journal on Scientific Computing*, 38(2):B219–B246, 2018. [2](#)
- [10] J. H. Bramble and J. T. King. A finite element method for interface problems in domains with smooth boundaries and interfaces. *Advances in Computational Mathematics*, 6(1):109–138, 1996. [2](#)
- [11] E. Burman, P. Hansbo, and M.G. Larson. A cut finite element method with boundary value correction for the incompressible stokes equations. pages 183–192, 2017. [2](#)
- [12] E. Burman, P. Hansbo, and M.G. Larson. A cut finite element method with boundary value correction. *Mathematics of Computation*, 87(310):633–657, 2018. [2](#)
- [13] Z. Cai, C. He, and S. Zhang. Discontinuous finite element methods for interface problems: Robust a priori and a posteriori error estimates. *SIAM Journal on Numerical Analysis*, 55(1):400–418, 2017. [2](#)
- [14] Z. Cai, X. Ye, and S. Zhang. Discontinuous galerkin finite element methods for interface problems: A priori and a posteriori error estimations. *SIAM Journal on Numerical Analysis*, 49(5):1761–1787, 2011. [2](#)
- [15] G. Chen and X. Xie. A robust weak Galerkin finite element method for linear elasticity with strong symmetric stresses. *Computational Methods in Applied Mathematics*, 16(3):389–408, 2016. [3](#), [8](#)
- [16] H. Chen, J. Li, and W. Qiu. Robust a posteriori error estimates for HDG method for convection–diffusion equations. *IMA Journal of Numerical Analysis*, 36(1):437–462, 2015. [3](#)
- [17] H. Chen, P. Lu, and X. Xu. A robust multilevel method for hybridizable discontinuous Galerkin method for the Helmholtz equation. *Journal of Computational Physics*, 264:133–151, 2014. [3](#)
- [18] Z. Chen and J. Zou. Finite element methods and their convergence for elliptic and parabolic interface problems. *Numerische Mathematik*, 79(2):175–202, 1998. [2](#), [4](#)
- [19] B. Cockburn, J. Gopalakrishnan, and R. Lazarov. Unified hybridization of discontinuous Galerkin, mixed, and continuous Galerkin methods for second order elliptic problems. *SIAM Journal on Numerical Analysis*, 47(2):1319–1365, 2009. [3](#)
- [20] B. Cockburn, J. Gopalakrishnan, and N. C. Nguyen. Analysis of HDG methods for Stokes flow. *Mathematics of Computation*, 80(274):723–760, 2011. [3](#)
- [21] B. Cockburn, N. C. Nguyen, and J. Peraire. A comparison of HDG methods for Stokes flow. *Journal of Scientific Computing*, 45(1):215–237, 2010. [3](#)
- [22] B. Cockburn, W. Qiu, and M. Solano. A priori error analysis for HDG methods using extensions from subdomains to achieve boundary conformity. *Mathematics of Computation*, 83(286):665–699, 2014. [3](#)
- [23] B. Cockburn and F.-J. Sayas. Divergence-conforming HDG methods for Stokes flows. *Mathematics of Computation*, 83(288):1571–1598, 2014. [3](#)

- [24] B. Cockburn and K. Shi. Superconvergent HDG methods for linear elasticity with weakly symmetric stresses. *IMA Journal of Numerical Analysis*, 33(3):747–770, 2013. 3
- [25] B. Cockburn and M. Solano. Solving dirichlet boundary-value problems on curved domains by extensions from subdomains. *SIAM Journal on Scientific Computing*, 34(1):A497–A519, 2012. 3
- [26] B. Cockburn and M. Solano. Solving convection–diffusion problems on curved domains by extensions from subdomains. *Journal of Scientific Computing*, 59(2):512–543, 2014. 3
- [27] H. Dong, B. Wang, Z. Xie, and L. L. Wang. An unfitted hybridizable discontinuous Galerkin method for the poisson interface problem and its error analysis. *IMA Journal of Numerical Analysis*, 37(1):444–476, 2016. 3
- [28] M. Dufloot. The extended finite element method in thermoelastic fracture mechanics. *International Journal for Numerical Methods in Engineering*, 74(5):827–847, 2008. 2
- [29] H. Gao, Y. Huang, and F. F. Abraham. Continuum and atomistic studies of intersonic crack propagation. *Journal of the Mechanics and Physics of Solids*, 49(9):2113–2132, 2001. 2
- [30] L. V. Gibiansky and O. Sigmund. Multiphase composites with extremal bulk modulus. *Journal of the Mechanics and Physics of Solids*, 48(3):461–498, 2000. 2
- [31] Y. Gong, Z. Li, and D. Gaffney. Immersed interface finite element methods for elasticity interface problems with non-homogeneous jump conditions. *Numerical Mathematics: Theory, Methods and Applications*, 46(1):472–495, 2010. 3
- [32] J. Guzmán and M. Olshanskii. Inf-sup stability of geometrically unfitted Stokes finite elements. *Mathematics of Computation*, 87(313):2091–2112, 2018. 2
- [33] C. Grkan, M. Kronbichler, and S. Fernandez-Mendez. eXtended hybridizable discontinuous Galerkin with heaviside enrichment for heat bimaterial problems. *Journal of Scientific Computing*, 72(2):542–567, 2017. 3
- [34] C. Grkan, E. Sala-Lardies, M. Kronbichler, and S. Fernandez-Mendez. eXtended hybridizable discontinuous Galerkin (X-HDG) for void problems. *Journal of Scientific Computing*, 66(3):1313–1333, 2016. 3
- [35] Y. Han, H. Chen, X. Wang, and X. Xie. EXtended HDG methods for second order elliptic interface problems. *arXiv preprint arXiv:1910.09769*, 2019. 3
- [36] A. Hansbo and P. Hansbo. An unfitted finite element method, based on Nitsches method, for elliptic interface problems. *Computer Methods in Applied Mechanics & Engineering*, 191(47-48):5537–5552, 2002. 2
- [37] A. Hansbo and P. Hansbo. A finite element method for the simulation of strong and weak discontinuities in solid mechanics. *Computer Methods in Applied Mechanics & Engineering*, 193(33):3523–3540, 2004. 2, 3
- [38] J. Huang and J. Zou. Some new a priori estimates for second-order elliptic and parabolic interface problems. *Journal of Differential Equations*, 184(2):570–586, 2002. 2
- [39] H. J. Jou, P. H. Leo, and J. S. Lowengrub. Microstructural evolution in inhomogeneous elastic media. *Journal of Computational Physics*, 131(1):109–148, 1997. 2
- [40] C. Lehrenfeld and A. Reusken. Optimal preconditioners for Nitsche-XFEM discretizations of interface problems. *Numerische Mathematik*, 135(2):1–20, 2016. 2
- [41] P. H. Leo, J. S. Lowengrub, and Q. Nie. Microstructural evolution in orthotropic elastic media. *Journal of Computational Physics*, 157(1):44–88, 2000. 2
- [42] R. J. Leveque and Z. Li. The immersed interface method for elliptic equations with discontinuous coefficients and singular sources. *SIAM Journal on Numerical Analysis*, 31(4):1019–1044, 1994. 3
- [43] B. Li and X. Xie. Analysis of a family of HDG methods for second order elliptic problems. *Journal of Computational and Applied Mathematics*, 307:37–51, 2016. 3
- [44] B. Li and X. Xie. BPX preconditioner for nonstandard finite element methods for diffusion problems. *SIAM Journal on Numerical Analysis*, 54(2):1147–1168, 2016. 3
- [45] B. Li, X. Xie, and S. Zhang. Analysis of a two-level algorithm for HDG methods for diffusion problems. *Communications in Computational Physics*, 19(5):1435–1460, 2016. 3
- [46] H. Li, J. Li, and H. Yuan. A review of the extended finite element method on macrocrack and microcrack growth simulations. *Theoretical and Applied Fracture Mechanics*, 2018. 2
- [47] J. Li, M. J. Markus, B. I. Wohlmuth, and J. Zou. Optimal a priori estimates for higher order finite elements for elliptic interface problems. *Applied Numerical Mathematics*, 60(1):19–37, 2010. 2
- [48] Z. Li. The immersed interface method using a finite element formulation. *Applied Numerical Mathematics*, 27(3):253–267, 1998. 3
- [49] Z. Li and K. Ito. *The immersed interface method: numerical solutions of PDEs involving interfaces and irregular domains*, volume 33. SIAM, 2006. 3
- [50] T. Lin, Y. Lin, and X. Zhang. Partially penalized immersed finite element methods for elliptic interface problems. *SIAM Journal on Numerical Analysis*, 53(2):1121–1144, 2015. 3
- [51] T. Lin, D. Sheen, and X. Zhang. A locking-free immersed finite element method for planar elasticity interface problems. *Journal of Computational Physics*, 247(16):228–247, 2013. 3

- [52] T. Lin and X. Zhang. Linear and bilinear immersed finite elements for planar elasticity interface problems. *Journal of Computational and Applied Mathematics*, 236(18):4681–4699, 2012. [3](#)
- [53] N. Moës, J. Dolbow, and T. Belytschko. A finite element method for crack growth without remeshing. *International Journal for Numerical Methods in Engineering*, 46(1):131–150, 1999. [2](#)
- [54] B. N. J. Persson and S. Gorb. The effect of surface roughness on the adhesion of elastic plates with application to biological systems. *Journal of Chemical Physics*, 119(21):11437–11444, 2003. [2](#)
- [55] M. Plum and C. Wieners. Optimal a priori estimates for interface problems. *Numerische Mathematik*, 95(4):735–759, 2003. [2](#)
- [56] F. Qin, J. Chen, Z. Li, and M. Cai. A cartesian grid nonconforming immersed finite element method for planar elasticity interface problems. *Computers & Mathematics with Applications*, 73(3):404–418, 2016. [3](#)
- [57] W. Qiu, J. Shen, and K. Shi. An HDG method for linear elasticity with strong symmetric stresses. *Mathematics of Computation*, 87(309):69–93, 2016. [3](#)
- [58] Y. Shen and A. Lew. An optimally convergent discontinuous Galerkin-based extended finite element method for fracture mechanics. *International Journal for Numerical Methods in Engineering*, 82(6):716–755, 2010. [2](#)
- [59] Y. Shen and A. Lew. Stability and convergence proofs for a discontinuous-Galerkin-based extended finite element method for fracture mechanics. *Computer Methods in Applied Mechanics & Engineering*, 199(37-40):2360–2382, 2010. [2](#)
- [60] O. Sigmund. Design of multiphysics actuators using topology optimization—Part II: Two-material structures. *Computer Methods in Applied Mechanics & Engineering*, 190(49-50):6605–6627, 2001. [2](#)
- [61] M. Solano and F. Vargas. A high order HDG method for Stokes flow in curved domains. *Journal of Scientific Computing*, 79(3):1505–1533, 2019. [3](#)
- [62] T. Strouboulis, I. Babuška, and K. Copps. The design and analysis of the generalized finite element method. *Computer Methods in Applied Mechanics & Engineering*, 181(1-3):43–69, 2000. [2](#)
- [63] A. P. Sutton and R. W. Balluffi. Interfaces in crystalline materials. 1995. [2](#)
- [64] P. F. Thomas and B. Ted. The eXtended/Generalized finite element method: An overview of the method and its applications. *International Journal for Numerical Methods in Engineering*, 84(3):253–304, 2010. [2](#)
- [65] T. Wang, C. Yang, and X. Xie. Extended finite element methods for optimal control problems governed by poisson equation in non-convex domains. *Science China Mathematics*, 61, 2019. [2](#)
- [66] H. Wu and Y. Xiao. An unfitted hp -interface penalty finite element method for elliptic interface problems. *arXiv preprint arXiv:1007.2893*, 2010. [7](#)
- [67] H. Wu and Y. Xiao. An unfitted hp -interface penalty finite element method for elliptic interface problems. 37(3):316–339, 2019. [7](#)
- [68] J. Xu. Estimate of the convergence rate of finite element solutions to elliptic equations of second order with discontinuous coefficients. *arXiv preprint arXiv:1311.4178*, 2013. [2](#), [4](#)
- [69] L. Zhang, A. Gerstenberger, X. Wang, and W. K. Liu. Immersed finite element method. *Computer Methods in Applied Mechanics & Engineering*, 193(21-22):2051–2067, 2004. [3](#)